HIGH SPEED CYLINDRICAL

ROLLER BEARING ANALYSIS

(NASA-CR-159460) HIGH SPEED CYLINDRICAL ROLLER BEARING ANALYSIS, SKF COMPUTER PROGRAM CYBEAN. VOLUME 1: ANALYSIS Final Report (SKF Industries, Inc.) 108 p HC A06/MF A01 CSCL 13I G3/37 N79-17222 Unclas 14092

SKF COMPUTER PROGRAM 'CYBEAN'

VOLUME I: ANALYSIS

JULY, 1978

R. J. Kleckner
J. Pirvics

SKF REPORT NO: AL78P022 SKF PROGRAM NO: AT78Y002

SUBMITTED TO:

NATIONAL AERONAUTICS & SPACE ADMINISTRATION
LEWIS CENTER
21000 BROOKPARK ROAD
CLEVELAND, OH 44135
UNDER CONTRACT NO. NAS3-20068

SUBMITTED BY:

SKF INDUSTRIES, INC.
TECHNOLOGY SERVICES DIVISION
1100 FIRST AVENUE
KING OF PRUSSIA, PA 19406

HIGH SPEED CYLINDRICAL ROLLER BEARING ANALYSIS

SKF COMPUTER PROGRAM 'CYBEAN'

VOLUME I: ANALYSIS

JULY, 1978

R. J. Kleckner
J. Pirvics

Prepared: R. J. Kleckner.

Approved:

Released:

SKF REPORT NO: AL78P022

SKF PROGRAM NO: AT78Y002

SUBMITTED TO:

NATIONAL AERONAUTICS & SPACE ADMINISTRATION
LEWIS CENTER
21000 BROOKPARK ROAD
CLEVELAND, OH 44135
UNDER CONTRACT NO. NAS3-20068

SUBMITTED BY:

SKF INDUSTRIES, INC.
TECHNOLOGY SERVICES DIVISION
1100 FIRST AVENUE
KING OF PRUSSIA, PA 19406

TABLE OF CONTENTS

SECTION	TITLE	PAGE
I	INTRODUCTION	1
II	PROGRAM ARCHITECTURE	3
III	ANALYSIS	8
IV	CONCLUSIONS AND RECOMMENDATIONS	12
APPENDIX A	WORK STATEMENT	17
APPENDIX B	COORDINATE FRAME DEFINITIONS AND TRANSFORMATIONS	23
APPENDIX C	GEOMETRY DEFINITIONS	31
APPENDIX D	LUBRICANT PROPERTY MODELS	39
APPENDIX E	FORCES ACTING ON A ROLLING ELEMENT	42
APPENDIX F	FITTING OF NON-CIRCULAR RINGS INTO NON-CIRCULAR HOUSINGS	67
APPENDIX G	GOVERNING EQUATION SET AND SOLUTION ALGORITHM	73
APPENDIX H	BEARING FATIGUE LIFE CALCULATIONS	83
APPENDIX I	THERMAL MODEL	87
REFERENCES		100
ATTACHMENT 1 -	ROLLER BEARING SPECIFICATIONS	102

LIST OF FIGURES

NO.	TITLE	PAGE
SECTION II - PROGRAM ARCHITECTURE		
1	BASIC PROGRAM STRUCTURE	6
APPENDIX B - COORDINATE FRAME DEFINITIONS AND TRANSFORMATIONS		
B-1	CYLINDRICAL ROLLER BEARING INERTIAL COORDINATE FRAMES	29
B-2	CYLINDRICAL ROLLER BEARING COORDINATE FRAMES	30
APPENDIX C - GEOMETRY DEFINITIONS		
C-1	ROLLER GEOMETRY	34
C-2	ROLLER SLICE GEOMETRY DETAIL	35
C-3	RING GEOMETRY DETAIL	36
C-4	RING SLICE GEOMETRY DETAIL	37
C-5	CAGE GEOMETRY DETAIL	38
APPENDIX E - FORCES ACTING ON A ROLLING ELEMENT		
E-1	INNER RING AND ROLLER SLICE INTERACTION DETAIL	60
E-2	OUTER RING AND ROLLER SLICE INTERACTION DETAIL	61
E-3	CROSS SECTION THROUGH A CYLINDRICAL ROLLER BEARING HAVING A FLANGED INNER RING	62
E-4	ROLLER END-FLANGE CONTACT GEOMETRY	63
E-5	HYDRODYNAMIC FRICTION FORCES ON SLIDING DISKS	64
APPENDIX F - FITTING OF NON-CIRCULAR RINGS INTO NON-CIRCULAR HOUSINGS		
F-1	NON-CIRCULAR PROFILE DESCRIPTION	72
APPENDIX G - GOVERNING EQUATION SET AND SOLUTION ALGORITHM		
G-1	SOLUTION ALGORITHM FOR MULTIPLE FLANGE CONTACTS	80
APPENDIX I - THERMAL MODEL		
I-1	FLUID HEAT NODES	95
I-2	DIVIDED FLUID FLOW FROM NODE i	96
I-3	CONTACT GEOMETRY AND TEMPERATURES	99

LIST OF TABLES

NO.	TITLE	PAGE
APPENDIX D - LUBRICANT PROPERTY MODELS		
D1	LUBRICANT PROPERTIES OF FOUR OILS.....	41

FOREWORD

This, Volume I of the report "High Speed Cylindrical Roller Bearing Analysis," documents the analysis, program design and algorithm detail employed in the generation of the computerized analytic design tool CYBEAN. All efforts involved in the generation of the code were sponsored by the NASA-Lewis Research Center of Cleveland, Ohio, under the administration of the Fluid System Components Division. The technical monitor was Mr. H. Coe. The work was performed under Contract No. NAS3-20068 at SKF Industries, Inc., King of Prussia, Pennsylvania, during the period September, 1976 through July, 1978.

Technical project leadership was executed by Mr. R. J. Kleckner, with contributions from: Drs. V. Castelli and J. Pirvics, Messrs. W. J. Crecelius and M. Ragen and Ms. M. M. Dinon.

VOLUME I

HIGH SPEED CYLINDRICAL ROLLER BEARING ANALYSIS

I. INTRODUCTION

Engine performance which satisfies the anticipated efficiency, speed and specific thrust requirements for aircraft in the coming decade project increased demands on their component performance. Engines will be required to operate at higher temperatures and speeds and to do so while maintaining low overall mass and high structural integrity. Bearings in particular emerge as critical system design elements.

Temperatures, which will be increased to extract more of the available thermodynamic engine cycle efficiency, affect bearing performance by threatening the dimensional stability of the system. Thermally induced excursions in geometry must be compensated for within the original bearing design to avoid premature and possibly catastrophic system failure.

Engine shaft speeds will be increased to derive greater compressor efficiency. Increased speeds, however, accentuate centrifugal effects. Dominance in raceway loading is transformed from inner to outer rings. Failure to maintain loaded contact on the inner ring across the spectrum of operating speeds results in the increased hazard of roller skidding, unnecessary heat generation and unstable performance. Combined with increased shaft diameters, required by system stiffness, increased speed raises questions beyond the limits of currently available bearing design analysis. This is especially true for cylindrical rolling element bearings where the diameter (mm)-speed (rpm) product, DN, approaches 3.0×10^6.

Field experience supports the assessment that available understanding and design tools are inadequate. Roller deterioration in bearings operating in the noted DN regime provides the physical evidence. This deterioration indicates that roller skidding occurs in lightly loaded high speed applications. High bearing temperatures and erratic kinematic behavior contribute to bearing degradation. Further examination indicates that reliable bearing operation depends on the ability to quantitatively assess the extent to which rollers will skew and which of the available design parameters can be manipulated to control this particular roller orientation during operation.

The deficiency in current design analysis tools is that the anticipated engine performance demands require the understanding of behavior which has previously resided in the realm of secondary effects.

This emergence of effects from secondary to primary significance has dictated the construction of new analysis software. The impetus for such effort has been further accelerated by the high labor and material costs required for purely experimental hardware research.

This report details the work performed to permit computation of the behavior of cylindrical rolling element bearings under high speed and misaligned shaft conditions. The program objectives were posed to enable accurate roller skew prediction under a wide variety of design geometry and loading conditions. Emphasis was also placed on the accurate assessment of general geometric preload design. Finally, it was recognized that such detailed information was deceptive without an integral and system related thermal analysis.

The work statement contained in Appendix A details the specific objectives relating to this NASA sponsored project. The material which follows details the procedures used in attaining the stated goals and instructs the reader in the use of the generated computer program CYBEAN. The documentation is presented in two volumes. Volume I describes program architecture and follows with modular documentation detailing formulation and mathematics. Volume II is written as a User's Manual for CYBEAN. The reader is presented with material which guides sensible and accurate use of the program. Volume II appropriately references Volume I for algorithm background or the details of simulation mathematics.

II. PROGRAM ARCHITECTURE

CYBEAN has been structured to be a bearing analysis tool by the coordinated execution of modules which perform specific analytic tasks.

The basic structure of the program is seen in Figure 1. Computation economies are accomplished by placing constants in structure locations external to repetitive operations.

CYBEAN initiates computation with geometry, lubricant and material definitions. The first repetitive loop is entered immediately thereafter, addressing the computation of interactive geometry fits. Arbitrary housing and outer ring profile interactions are considered here. Load distribution and displacement values are obtained for the specific mode of bearing support specified by the user. The evaluation of the field equation set for a bearing which contains n_r rollers is now started.

The set of values for the independent variables which at a particular instant in time simultaneously satisfy all equations of equilibrium are considered to be a solution. These values are obtained by solving as many as $6n_r + 5$ simultaneous nonlinear equations using a Newton-Raphson algorithm.

The individual positions of the rolling elements within the complement at that instant are defined by reference to the orientation azimuth angle, ψ_1, of the first rolling element.

Because of the nature of the governing equation set, an accurate initial guess of the variable values would result in considerable savings in computer execution time. However, the nonlinear coupling of a large set of unknowns within the physical system creates difficulty in the generation of an accurate initial guess.

To overcome this problem and maintain computation time at an economic level, the simpler elastic problem is solved first. The set of variable values which satisfy the equilibrium of elastic forces are then used as an initial guess for the more complicated solution which includes friction. This solution is also used to determine the equilibrium load distribution which defines housing fit pressures. The basic problem is described by Liu [1], the number of degrees of freedom considered are $2n_r + 2$.

The general field equation set is partitioned prior to its evaluation and eventual solution. Independent variables describing the inner ring position and roller radial position are addressed in conjunction with field equations governing ring and roller radial equilibrium. Equation cross coupling is established through the roller radial position. This subset is brought to equilibrium by Newton-Raphson iteration.

Once inner ring equilibrium is satisfied, the field equation set is again partitioned to include roller axial, radial, skew and tilt moment equations of equilibrium. Coupling is maintained through the associated displacement variables. At this portion of the analysis, roller end flange contact forces are equilibrated with raceway induced loading.

A final partition is made such that the field equations defining force equilibrium in the z-direction, moments about the roller axis, radial and cage equilibrium are considered. Associated variables are: radial position, rotational and orbital speeds and cage displacements. That set of independent variables whose values simultaneously satisfy these equations is considered a solution.

Satisfactory convergence of the iterative procedure allows the definition of results for a specific temperature. The remaining program structure addresses the computation of steady state and the time transient thermal performance of the system.

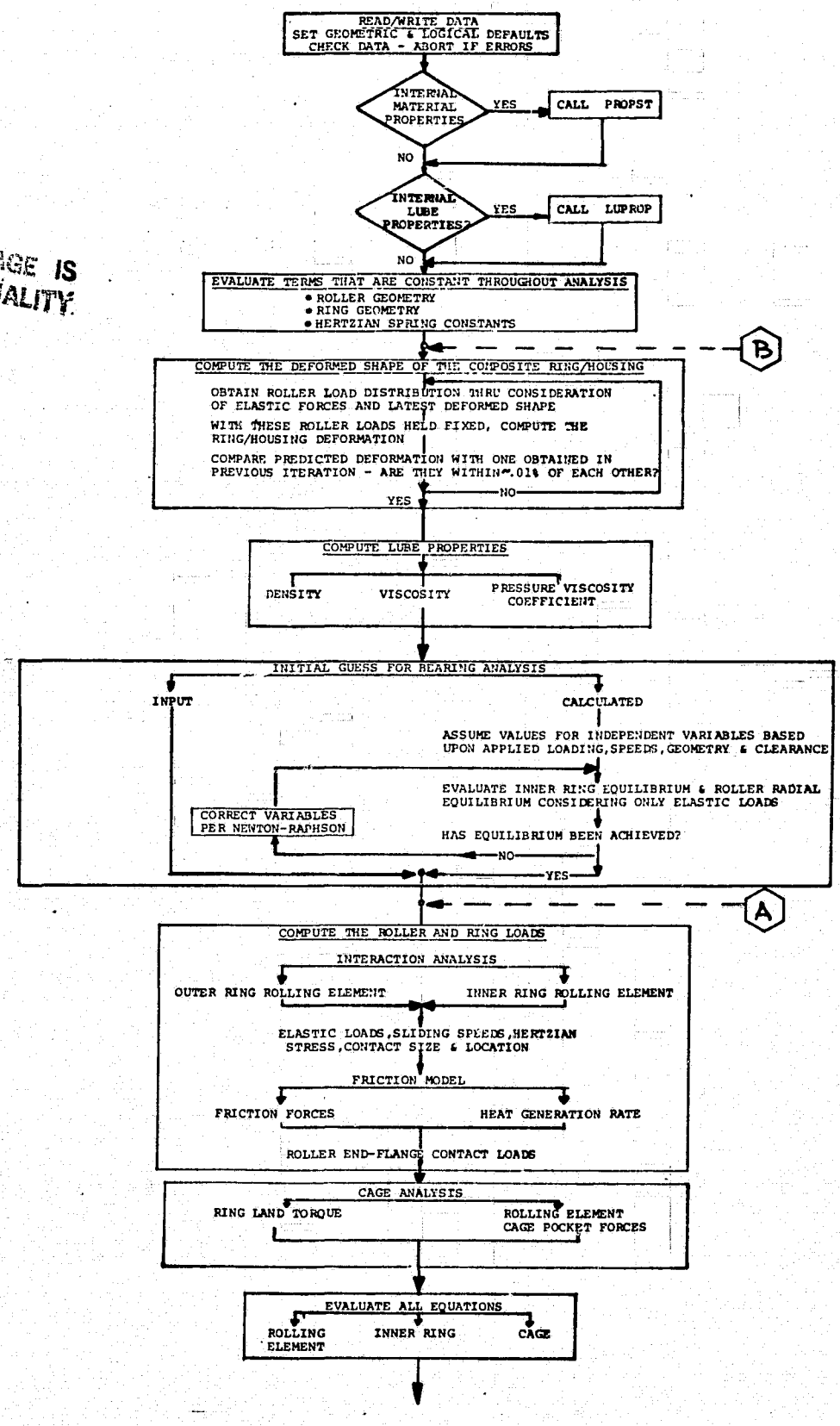

FIGURE 1: BASIC PROGRAM STRUCTURE

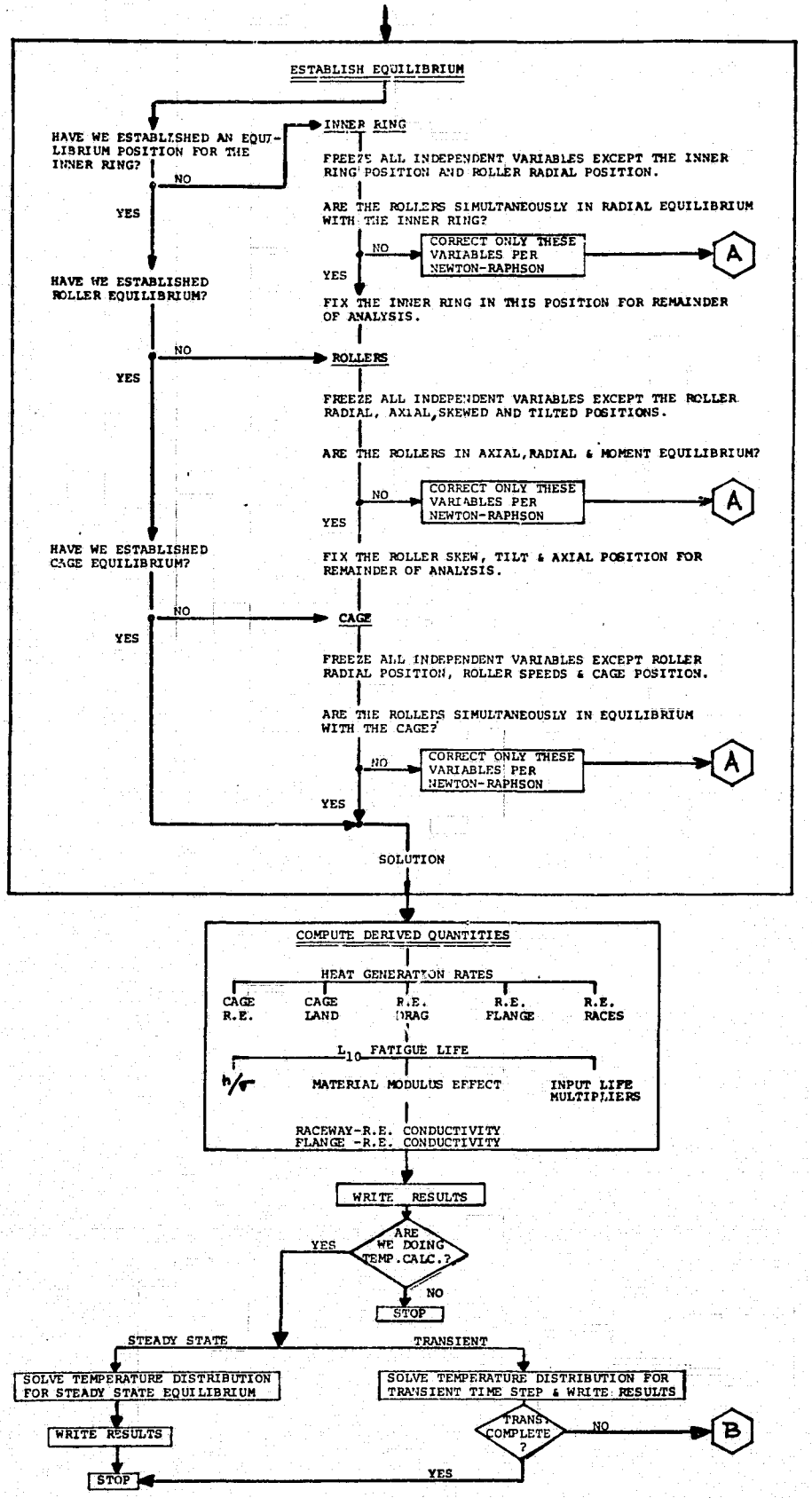

FIGURE 1 (CONT'D): BASIC PROGRAM STRUCTURE

III. ANALYSIS

The preceding description of program architecture serves to provide an overview of CYBEAN structure. The analysis represented by this computation algorithm is described in the material which follows.

The bulk of the calculations performed address repetitive computation of displacements and forces resulting from solid-solid and solid-fluid interactions. These interactions are permitted to occur in a thermally varying environment and are viewed as part of a system in quasi-static thermodynamic equilibrium. The system is defined by geometric and material description of the bearing complement and the rheology of the lubricant used. It is considered to be driven by an external forcing function which consists of a constant vector set representing definitions of shaft rotation, speed and applied radial force. Additional system stimulation is accepted from heat generated within the boundaries of the defined system volume.

The analysis consists of an ordered series of mathematical descriptions which detail the piecewise and ultimately continuous equilibrium achieved by the system in response to the applied forcing function. It describes the response of the system in terms of force, displacement and temperature distributions.

The bearing analysis is initiated through the definition of the coordinate space in which it is described. An inertial reference frame, chosen to be coincident with an inner ring reference frame when the bearing is unloaded, is established such that its X-axis defines the bearing longitudinal centerline. Each element is then assigned a moving coordinate frame. For the rollers, this frame is coincident with an analogous inertial frame when the bearing is unloaded. Thus defined, a general displacement (composed of both translation and rotation) of any bearing component can be written in the terms of a coordinate

transformation from its inertial reference frame. Six coordinates for a given transformation are required to establish the displaced positions of each bearing component. However, if axial symmetry exists constraining assumptions can be imposed on the nature of the displacement, and the number of degrees of freedom required to define the rigid body displacements can be reduced. Specifically:

Inner Ring - The study of misalignment effects on bearing performance is made convenient by the ability to define the misalignment angle. An additional constraint on the axial displacement and the presence of rotational symmetry can reduce the degrees of freedom to two. Thus, a very restricted representation describes translation of the ring within its radial plane.

Cage - Motion can be restricted as with the inner ring, although rotation is permitted about its longitudinal axis.

Rollers - Axial symmetry and the recognition that translation in the direction tangent to the pitch circle is negligibly small can limit the motion to 4 degrees of freedom.

Those quantities which define the degrees of freedom through which the coordinate frames may move form a subset of the independent variables in the field equation set. The complete set includes the roller rotational and orbital speeds.

The definition of general coordinate space transformations and the general geometric description of each element in the bearing complement (within its particular coordinate frame) eases the formulation and permits flexibility in the numerical experimentation required to attain optimum solution algorithms. Appendix B details this basic transform structure.

The effort has been directed at formulating the description to allow full generality. This modular freedom is guaranteed by the automated coupling provided by the transformations noted above.

The geometric characterization of rings, rollers and cage is elaborated upon in Volume II of this work. Some of the figures used in Volume II are repeated here, in Appendix C.

To introduce physical significance, spacial definition of the system and its components requires characterization by specific material properties and lubricant rheology.

Solids are characterized as linearly elastic deforming materials whose properties are temperature independent. Specific material properties are found in Volume II.

Lubricating fluid is characterized as having properties that vary with both temperature and pressure. Models used to evaluate properties are shown in Appendix D.

Once geometry and material properties are defined specific interaction mechanisms must be described to formulate the force equilibrium field equation set. Two major descriptive areas arise: solid-solid and solid-fluid interactions.

The solid-solid interaction is characterized as follows: given a set of values for the independent variables, positions of all the bearing components are established in space. With these positions fixed, the relative positions of the bearing components are examined to determine if the bodies contact or a free space exists between them. Locations and magnitudes of interpenatration are recorded. These values are subsequently used to determine contact stress, contact size and the associated elastic force.

The solid-fluid interaction occurs in four ways: raceway/rolling element traction, flange/rolling element traction, roller drag and cage related friction. Again, with the positions and speeds fixed, these effects can be computed for the raceway using established models. In this work, models used to treat flange/rolling element and raceway/rolling element interactions are identical. Roller drag is approximated as a function of lubricant properties, speed and geometry, using established equations for external flow. These interactions and the cage model are detailed in Appendix E.

The analysis of induced preload through variable geometry ring interactions with a variable geometry housing is described in Appendix F.

The completion of the description detailing interaction mechanisms allows the generation of the quasidynamic force equilibrium equations and attendant strategies for solution. A Newton-Raphson iterative procedure noted in the preceding section is used. Modification of the equation set through the incorporation of kinematic equations is detailed in Appendix G.

The culmination of the iteration procedure which satisfies the quasidynamic equilibrium field equation set permits the display of values for the vector of unknowns and the computation of bearing fatigue life. The latter is computed according to standard Lundberg-Palmgren methods detailed in Appendix H.

The description to this point has addressed the bearing analysis performed at a given set of component temperatures. Thermal effects can be computed in either of two modes.

The first mode details the steady state operating temperatures of the bearing and its environment. CYBEAN will formulate the conservation of energy equations for an equivalent nodal model of the bearing and surrounding hardware. This model is prepared by the user according to methods shown in Volume II. Equations are solved for the steady state temperature distribution.

The second mode details time transient effects. Here, CYBEAN solves a system of first order nonlinear differential equations. Typically, initial values are taken as the solution to the steady state analysis. Modelling assumptions are presented in Appendix I, and also Volume II of this work.

IV. CONCLUSIONS AND RECOMMENDATIONS

The material presented in the preceding chapters documents the creation of the state of the art high speed cylindrical rolling element bearing analysis/design tool CYBEAN. The formulations are general and the program architecture modular to permit easy maintenance and expansion.

The current edition of CYBEAN enables detailed examination of bearing performance and in particular permits exploration of causes for and consequences of bearing skew. The very general capability for calculation of geometrically induced preload allows design assessment of bearings for engine mainshaft support. The integral thermal analysis capability obsoletes previous isothermal computation algorithms for state of the art 3×10^6 DN bearing application investigations.

During the course of the work performed, a perspective was gained on the additional requirements for the accurate simulation of design components for future generation engines. These requirements relate to the previously noted emergence of physical phenomena from secondary to primary effect significance as operating conditions specify higher speeds and temperatures. Proper assessment of influence on bearing performance demands an investment in basic analytic formulation and corresponding detailed experimental verification. It is specifically recommended that:

1. The EHD model be reformulated. Experiments leading to the current version, developed in the early 1970's, excluded regimes which are forecast for the 1980's. This inadequacy is experienced when performance includes a high degree of skidding.

2. The effects of lubricant distribution be investigated. Thermal/dimensional stability and thus power loss in a bearing is exceptionally sensitive to the assumptions concerning the lubricant distribution within the bearing cavity. This sensitivity is accentuated with increased speed and temperature. Both of these parameters have increasing effects with bearing operation at elevated DN values.

3. Surface traction effects be related directly to material failure and thus bearing failure predictions.

4. The microscale topography of surfaces be quantified in three dimensions to enable rational formulation of upgraded EHD models which address physical events in this microscale realm. Current procedures are limited by excessive measurement times and mechanical filtering within the frequencies of interest.

5. The mathematics of numerical methods be more fully expolited to enable economically justifiable computation in parametric explorations.

6. Extensive work be performed to obtain a quantitative understanding of phenomena associated with partial film and lost lubrication operating conditions.

The current edition of CYBEAN as well as the state of the art itself would benefit from investigations in any and all of the six items noted above. In addition, specific immediate modifications and capability expansions for CYBEAN warrant attention. These are represented as the following tasks:

1. Expand CYBEAN to accept external shaft applied axial load.

2. Expand CYBEAN to couple with a shaft and another rolling element bearing.

3. Expand the fit routines to accomodate hoop strain.

4. Modify CYBEAN to enable temperature dependent material property definition.

5. Modify CYBEAN to automate the partitioning algorithm to respond to operating vector extremes.

6. Expand CYBEAN to contain line plotter printing capability for time transient run information display.

7. Expand CYBEAN to include a generalized interative thermoelastic outer ring housing description.

In conclusion a recommendation is made for the expanded parametric exercise and documentation of obtained results. These results and the current edition of CYBEAN should be incorporated within a design guide for cylindrical rolling elements to provide a practical tool for the designer and analyst of reliable aircraft engine bearings operating in and beyond the 3×10^6 DN regime.

APPENDIX A

WORK STATEMENT

VOLUME I

APPENDIX A: WORK STATEMENT

The Contractor shall furnish the necessary personnel, materials, services, facilities, and otherwise do all things necessary for or incident to the completion of the work set forth below:

Task I - Program Development

The Contractor shall design, develop and furnish a fully operational computer program that will predict the performance characteristics of high-speed cylindrical roller bearings, with the following requirements:

A. All the capabilities present in the bearing subprogram contained in SKF computer program No. AT76Y001 currently installed at NASA-Lewis Research Center shall be contained in this new program.

B. The new program shall contain a "Roller Skew Analysis" wherein each roller shall be permitted to skew and this skew shall be resisted by flanges on either the inner or outer ring.

C. Allowable program input shall include distinct roller-end spherical radius, flange angle, flange profile radius and roller-flange axial play.

D. Each roller shall per permitted six degrees of freedom-these are:

1. Radial displacement
2. Axial displacement
3. Angular displacement about the roller Z axis (Roller Tilt)
4. Angular displacement about the roller Y axis (Roller Skew)
5. Rotational speed (about roller X-axis)
6. Orbital speed (about bearing center)

E. The bearing shall be permitted to have a complement of up to 50 rollers.

F. The computation of the set of values of the variables in I-D that results in roller quasidynamic equilibrium shall be calculated through consideration of the elastic and friction forces imparted to each roller by the raceways, free lubricant, cage, and by the ring flanges. Inertial loads shall also be considered.

G. Important parameters such as EHD film thickness and Hertz stress shall be determined for each roller end-flange contact.

H. Inasmuch as certain computations will be similar to previous programs, existing subroutines shall be used as much as possible. In particular, the following SKF subroutines shall be available for use with the new program:

PROPST, LUPROP, LUBCON, GUESCG, FIT, INTFIT, SIMEQ, SOLVXX, INSOLV, PARDER, EQCHEK, EQWRIT, ERCHEK, LIFE, LRHS, BOT, VISCOZ, ALPHAO, DRAGNO, STCON, STARFC, HOHI, HDFRIC, HRFRIC, EHDSKF, FRICTN, NASEHD, DRAG, CAGESP, CAGEQ, CGLAND, CGWET, CGRE, CGBALI, CGNRMN, CGEHDD, CGHDP, CGFRN, CGHDF, CGEHF, SUMCGL, SUMRE, BRCAX, BRAX, TEMPIN, INPUM, RWHTC, RWGRWHC, TMAP, NET, NETEET and STEPLMA.

I. The computer program shall be capable of treating each of the following four methods of using flexible out-of-round bearing ring designs to induce roller preload.

1. The outer ring has an elliptical OD and a variable wall thickness (round ID).

2. The outer ring has an elliptical OD and a uniform wall thickness (elliptical ID).

3. The outer ring has a round OD and a variable wall thickness (elliptical ID).

4. The outer ring has a three-lobed OD and ID with a uniform wall thickness.

J. The new program shall be designed for eventual installation into the SHABERTH/NASA SKF Shaft-Bearing Computer Program No. AT76Y001 as a subprogram module.

K. The program shall include a capability to predict steady state and transient thermal performance of the roller bearing system.

1. The mechanical performance analyses shall interact with the temperature mapping-heat dissipation analyses so that

(a) The computed bearing component temperatures will influence bearing diametral clearances

(b) The computed lubricant temperatures will influence lubricant viscosity, density and pressure-viscosity coefficient and

(c) The calculated bearing frictional heat generation will influence the thermal analysis.

2. The thermal analysis shall include the capability for calculation of roller-raceway and roller-flange heat transfer coefficients.

Task II - Program Demonstration

The Contractor shall demonstrate the use of the program developed in Task I by performing a computer analysis of a cylindrical roller bearing having specifications and operating conditions as described in Attachment 1.

A. The purpose of the first study shall be primarily to demonstrate the ability of the program to predict roller skew and the resulting roller-end, flange interactions. Therefore, to accomplish this, two sets of roller end, flange geometry shall be examined under a condition of aligned and misaligned bearing rings, as noted in Attachment 1. The thermal analysis shall not be used in this study.

B. The purpose of the second study shall be primarily to demonstrate the ability of the program to predict roller bearing performance as a function of the calculated temperatures. The steady state thermal analysis shall be used. To accomplish this, one set of roller end, flange geometry shall be examined under one condition of aligned and one condition of misaligned bearing rings as noted in Attachment 1.

Task III - Program Installation

The computer program shall be installed on the UNIVAC 1100/40 computer at the NASA Lewis Research Center.

A. The Contractor shall supply a program user's manual which will demonstrate and review program input, output, structure and solution methods.

B. The Contractor shall supply one copy of the program source listing.

C. The program's satisfactory installation at Lewis will be confirmed when the source program supplied by the Contractor has been successfully compiled, and executed, and the output correlated with the results of a test case (one of the data points from Task II) provided by the Contractor.

D. As part of the requirement of this contract, the Contractor shall provide qualified technical assistance for a period not to exceed forty (40) engineering man-hours, to advise the Lewis Project Manager of any deficiency which may preclude proper operation, in the NASA-Lewis Research Center computer, of the computer program to be delivered hereunder.

Task IV - Reporting Requirements

Technical, schedular, and financial reporting shall be in accordance with the Reports of Work attachment (with NASA Forms 533M and 533P) which is hereby made a part of this contract except as modified below:

A. The number of report copies to be submitted is as follows:

1. Monthly Technical Report, a maximum of twelve (12) copies.

2. Contractor's Financial Management Performance Analysis Report (533P) (Blocks 1, 2, 6 and 11 only), maximum of twelve (12) copies.

3. Monthly Financial Management Report (NASA Form 533M), a maximum of four (4) copies. Column 8(a) shall contain the cost estimates for the month following that reported in column 7(a). Column 8(b) shall contain the cost estimates for the month following that reported in column 8(a).

B. The reporting categories to be reported on the Contractor's Monthly reports are as follows:

Reporting Category	Description
Task I	Program Development
Task II	Program Demonstration
Task III	Program Installation
Task IV	Reports

C. Both costs and hours shall be reported for each category. Additional reporting categories shall be the following:

Total Contract Costs/Hours
Fee
Total Contract

The reporting using the Form 533P shall consist of columns 7(b) (Planned Value of Work Accomplished) and 11 (Technical Assessment of Progress). In column 7(b), all the above reporting categories shall be included, but only dollars are required. The same reporting categories shall be used in column 11, except that the last two categories above (i.e., Fee and Total Contract) shall be omitted.

D. The monthly reports submission date shall be within ten (10) operating days after the closing date of the Contractor's accounting month.

E. Within thirty (30) calendar days after notification of approval of the Contractor's proposed final report, the Contractor shall distribute a maximum of twenty (20) copies of the approved final report as directed in writing by the Contracting Officer. In addition, the Contractor shall furnish one (1) set of glossy photographs of all continuous tone figures included in the final report.

SPECIAL REQUIREMENTS

Computer Program Minimum Acceptance Standards

The computer program submitted in this contract shall be prepared for submission to NASA Lewis Research Center in accordance with the minimum standards of good practice for computer programming as defined below.

A. The program shall be written entirely in ANSI FORTRAN X3.9-1966 and compilable by the UNIVAC FORTRAN V compiler. Machine language functions or subroutines shall not be used that are not available on the standard FORTRAN V Library.

B. All subroutine and program options will be fully defined. Test input and results will be developed to demonstrate the normal program operation. Additional inputs and results will be supplied to demonstrate the use of each option.

C. The overall program should be written so as to keep the amount of operation card and tape handling to a minimum. Operating instructions must be clear. Instructions requiring halting of the machine, use of external sense switches, operator intervention or mounting of tapes after program has started execution are not permitted.

D. The program description shall include the following:

1. A complete definition and analysis of the problem including equations with engineering units.

2. A source listing of the program, subroutines, and functions.

3. A complete description of program capabilities, logical techniques and options.

4. A description of all known operational peculiarities, limiting cases, and accuracy levels including reasons for typical failures.

5. A list of all input and output parameters with corresponding units and formats.

APPENDIX B

COORDINATE FRAME DEFINITIONS AND TRANSFORMATIONS

VOLUME I

APPENDIX B: COORDINATE FRAME DEFINITIONS AND TRANSFORMATIONS

Consider a cylindrical rolling element bearing with a flanged inner ring, Figure B1. Introduce the coordinate system $(X,Y,Z)_o$ such that the X_o axis is coincident with the outer ring longitudinal centerline. The Y_o axis defines the angle $\psi = 0°$ and the Z_o axis $\psi = 90°$. The origin of the $(X,Y,Z)_o$ system is chosen such that the Y_o- Z_o plane bisects the outer ring roller path effective length. The $(X,Y,Z)_o$ system is fixed with respect to the outer ring, and the outer ring center of mass is fixed in space.

Introduce second and third moving coordinate systems, $(X,Y,Z)_I$ and $(x,y,z)_c$, initially coincident with $(X,Y,Z)_o$ but attached to the inner ring and cage respectively, and free to move through space with these components.

Introduce a fourth coordinate system $(x,y,z)_i$, at each roller location i. This will be referred to as the i-th roller inertial coordinate system, $(R)_i$. The origin of the $(x,y,z)_i$ system is along the roller axis and in the Y_o- Z_o plane, Figure B1. Note that the x_i axis is parallel with X_o and defines the roller axis; y_i is directed radially outward and z_i is tangent to the pitch circle. The $(x,y,z)_i$ coordinate frame positions are fixed in space, relative to $(X,Y,Z)_o$.

Now introduce a fifth coordinate system $(\bar{x},\bar{y},\bar{z})_i$ which is initially coincident with the $(x,y,z)_i$ but is fixed with the roller and free to move through space with it. This frame will be referred to as the roller frame $(\bar{R})_i$, Figure B2.

GENERAL FORM OF THE ORTHAGONAL TRANSFORM

It is frequently necessary to express the components of a given vector in at least two coordinate frames. This is particularly so in definitions of geometry. Here, initial specification is convenient in inertial coordinate frames. However, the analysis which follows frequently requires redefinition in frames which are in motion.

The linear orthagonal transformation operator [2], $[\Phi TS]$, describes the rotation portion of transformation from the "S" coordinate system to the "T" coordinate system. It can be written as:

$$[\Phi TS] = \phi^{TS}_{k,\ell} \quad ,$$

where $k = 1,2,3$ and $\ell = 1,2,3$.

The most general transformation between Cartesian coordinate systems is composed of a rotation and translation. Under translation, the coordinates of a point described relative to both systems will differ merely by a constant vector, which may be defined in either coordinates. The transformation of a vector $\{\bar{P}\}_S$ whose terminus locates the point P in the "S" coordinate frame to a vector $\{\bar{P}\}_T$ whose terminus locates the same point P in the T coordinate frame can be written as

$$\{\bar{P}\}_T = [\Phi TS]\{\{\bar{P}\}_S + [\Phi D]\ \{\bar{U}\}_E\}_S \qquad (1)$$

where $\{\bar{U}\}_E$ is the constant vector describing the translation portion of the transformation, and $[\Phi D]$ is a second rotation transformation operator.

If the vector $\{U\}_E$ in equation (1) is expressed in the final coordinate frame, i.e. E=T, then

$$[\Phi D] = [\Phi TS]^{-1} \tag{2}$$

However, the reciprocal matrix is the transposed matrix

$$[\Phi D] = [\tilde{\Phi}TS] \tag{3}$$

If translation is specified in the final frame, equations (3) and (1) are combined to give:

$$\{\bar{P}\}_T = [\Phi TS]\ \{\bar{P}\}_S + \{\bar{U}\}_T \tag{4}$$

Conversely, if translation is specified in the initial coordinate frame, i.e. E=S, then

$$[\Phi D] = [I] \tag{5}$$

and

$$\{\bar{P}\}_T = [\Phi TS]\ \{\bar{P} + \bar{U}\}_S \tag{6}$$

Here, I is the identity matrix.

Six general transformations need to be related to the independent variables:

1. Roller inertial (R) coordinate frame to the roller ($\bar{R}$) coordinate frame, $[\Phi\bar{R}R]$.
2. Outer ring (O) coordinate frame to the roller (R) coordinate frame, $[\Phi RO]$.
3. Inner ring (I) coordinate frame to the outer ring (O) coordinate frame, $[\Phi OI]$.

4,5,6. Inverse transformations of 1, 2, and 3.

Consider transformation between the roller and roller inertial frames. Four parameters specify the displacement of the roller. They are: two components of translation (u_x and u_y), and, two angles of rotation γ_y (roller skew) and γ_z (roller tilt).

In terms of the angles of rotation of the i-th roller, γ_{y_i} and γ_{z_i}, we obtain:

$$[\Phi\bar{R}R] = \begin{bmatrix} \cos\gamma_{z_i} & \sin\gamma_{z_i} & 0 \\ -\sin\gamma_{z_i} & \cos\gamma_{z_i} & 0 \\ 0 & 0 & 1 \end{bmatrix} \cdot \begin{bmatrix} \cos\gamma_{y_i} & 0 & -\sin\gamma_{y_i} \\ 0 & 1 & 0 \\ \sin\gamma_{y_i} & 0 & \cos\gamma_{y_i} \end{bmatrix}$$

which, after expansion, reduces to

$$[\Phi\bar{R}R] = \begin{bmatrix} \cos\gamma_{z_i} & \cos\gamma_{y_i} & \sin\gamma_{z_i} & -\sin\gamma_{y_i}\cos\gamma_{z_i} \\ -\sin\gamma_{z_i} & \cos\gamma_{y_i} & \cos\gamma_{z_i} & \sin\gamma_{y_i}\sin\gamma_{z_i} \\ \sin\gamma_{y_i} & & 0 & \cos\gamma_{y_i} \end{bmatrix}$$

The inverse transformation is given by:

$$[\tilde{\Phi}\bar{R}R] = [\Phi R\bar{R}] = \begin{bmatrix} \cos\gamma_{z_i} & \cos\gamma_{y_i} & -\sin\gamma_{z_i} & \cos\gamma_{y_i} & \sin\gamma_{y_i} \\ \sin\gamma_{z_i} & & \cos\gamma_{z_i} & & 0 \\ -\sin\gamma_{y_i} & \cos\gamma_{z_i} & \sin\gamma_{y_i} & \sin\gamma_{z_i} & \cos\gamma_{y_i} \end{bmatrix} \quad (8)$$

Similarly, we obtain these values for the four remaining transformation operators:

$$[\Phi RO]_i = \begin{bmatrix} 1 & 0 & 0 \\ 0 & \cos\psi_i & \sin\psi_i \\ 0 & -\sin\psi_i & \cos\psi_i \end{bmatrix} \quad (9)$$

$$[\Phi OR]_i = \begin{bmatrix} 1 & 0 & 0 \\ 0 & \cos\psi_i & -\sin\psi_i \\ 0 & \sin\psi_i & \cos\psi_i \end{bmatrix} \quad (10)$$

$$[\Phi OI] = \begin{bmatrix} \cos\gamma_{z_i}\cos\gamma_{y_i} & -\sin\gamma_{z_i}\cos\gamma_{y_i} & \sin\gamma_{y_i} \\ \sin\gamma_{z_i} & \cos\gamma_{z_i} & 0 \\ -\cos\gamma_{z_i}\sin\gamma_{y_i} & \sin\gamma_{z_i}\sin\gamma_{y_i} & \cos\gamma_{y_i} \end{bmatrix} \quad (11)$$

$$[\Phi IO] = \begin{bmatrix} \cos\gamma_{z_i}\cos\gamma_{y_i} & \sin\gamma_{z_i} & -\cos\gamma_{z_i}\sin\gamma_{y_i} \\ -\sin\gamma_{z_i}\cos\gamma_{y_i} & \cos\gamma_{z_i} & \sin\gamma_{z_i}\sin\gamma_{y_i} \\ \sin\gamma_{y_i} & 0 & \cos\gamma_{y_i} \end{bmatrix} \quad (12)$$

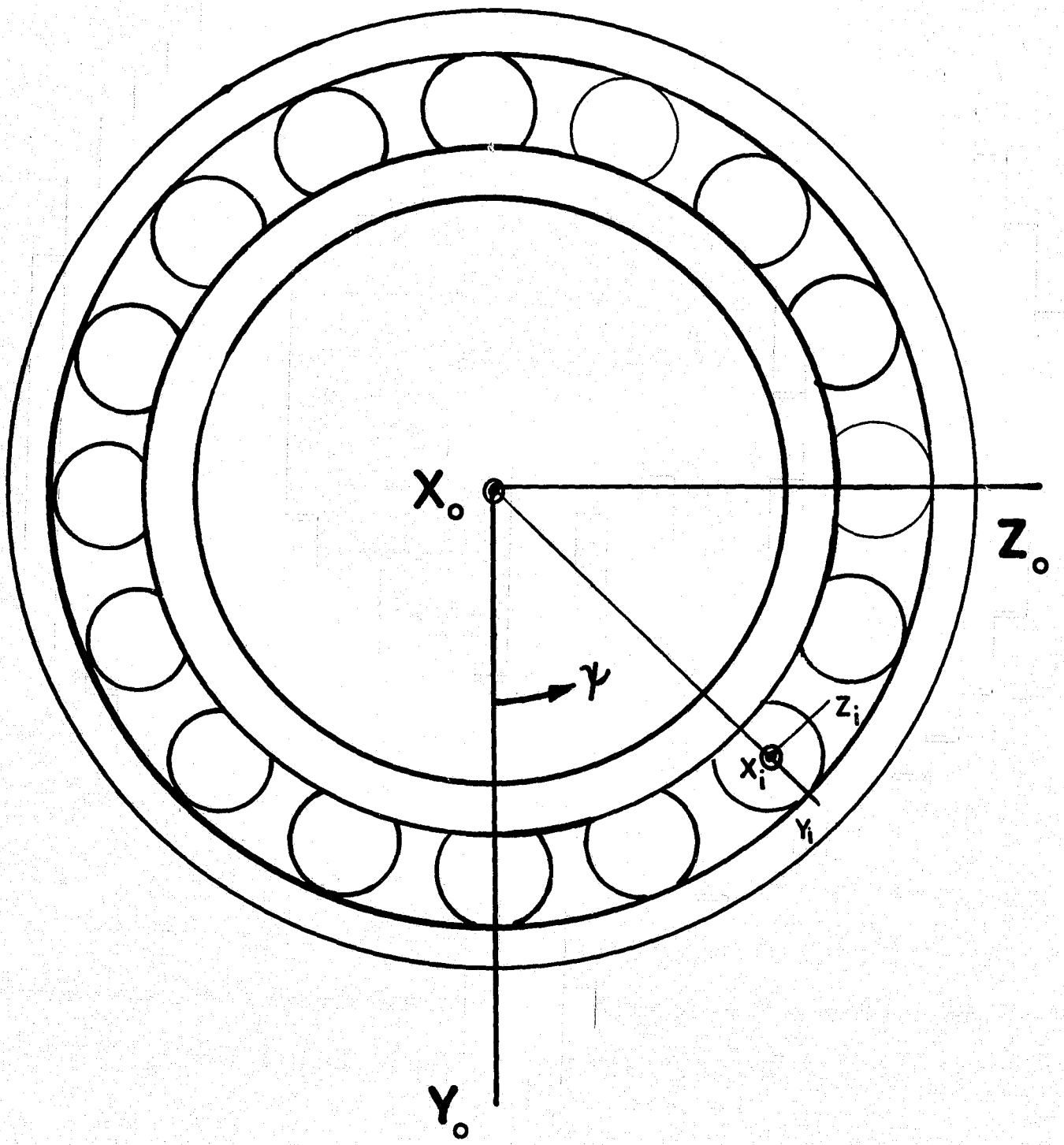

FIGURE B1: CYLINDRICAL ROLLER BEARING INERTIAL COORDINATE FRAMES

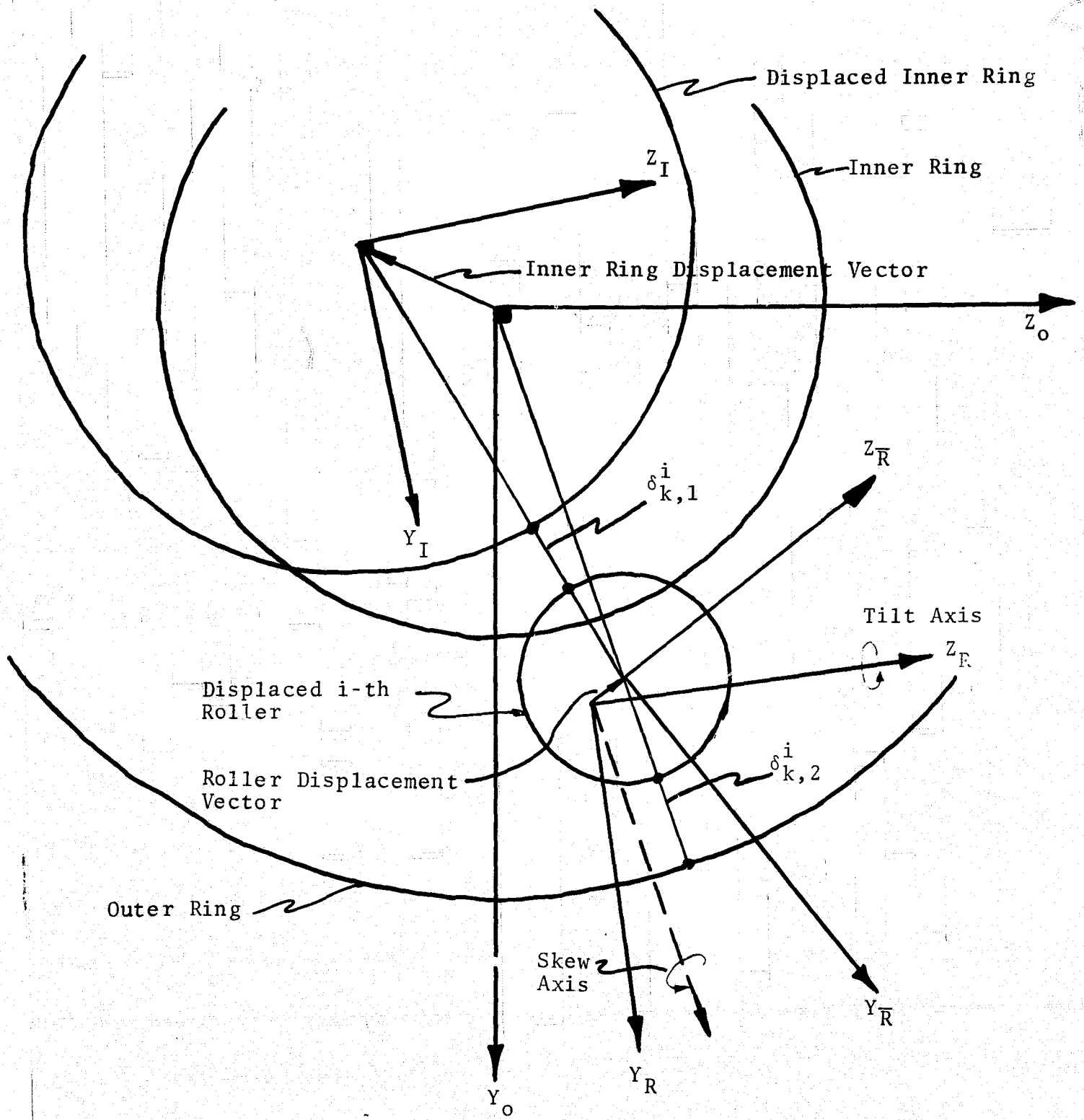

FIGURE B2: CYLINDRICAL ROLLER BEARING COORDINATE FRAMES.

APPENDIX C

GEOMETRY DEFINITIONS

VOLUME I

APPENDIX C: GEOMETRY DEFINITIONS

It is essential to the analysis that the geometries of the interacting solids are described as accurately as possible. This accuracy has to be maintained in parallel with description generality.

ROLLER GEOMETRY

Analysis requires that the roller geometry be represented as a composite of slices which have finite width and radius. These radii are computed as functions of roller data. In the nomenclature of Figure C1 the k-th roller slice radius is given at $x = \bar{x}$ by

$$R_k = D_{EFF} - C_r \left(1 - \cos\{\sin^{-1} \left(\frac{\bar{x}}{C_r}\right)\}\right) \tag{1}$$

in the crowned zone, and by

$$R_k = D/2 \tag{2}$$

in the flat region. Here,

$$D_{EFF} = C_r + \frac{D}{2} - \left(C_r^2 - (\ell_0/2)^2\right)^{\frac{1}{2}}. \tag{3}$$

Originally, these radii may be individually specified for a completely arbitrary roller geometry. Figure C2 shows eight radii which define the geometry of a typical roller. Seven "slices" were used in this example. Up to 21 radii and 20 slices may be specified.

RING GEOMETRY

As with the roller geometry, analysis requires that the ring geometry be specified in the same "sliced" format.

In the nomenclature of Figure C3, the k-th ring slice radius is given at $x = \bar{x}$ by

$$R_{k,m} = \frac{1}{2}\left(D' \pm D \pm \frac{p_d}{2}\right) \pm G_m \left(1 - \cos\{\sin^{-1} \left(\frac{\bar{x}}{G_m}\right)\}\right) \tag{4}$$

Here, the upper sign refers to the outer race, the lower to the inner race and p_d to the diametral clearance.

Optionally, these radii may be directly specified for a completely arbitrary ring geometry. Figure C4 shows six radii which define the geometry of a typical raceway. Five slices were used in this example.

CAGE GEOMETRY

A minimum of information is required to define the cage geometry. The relevant dimensions are shown in Figure C5.

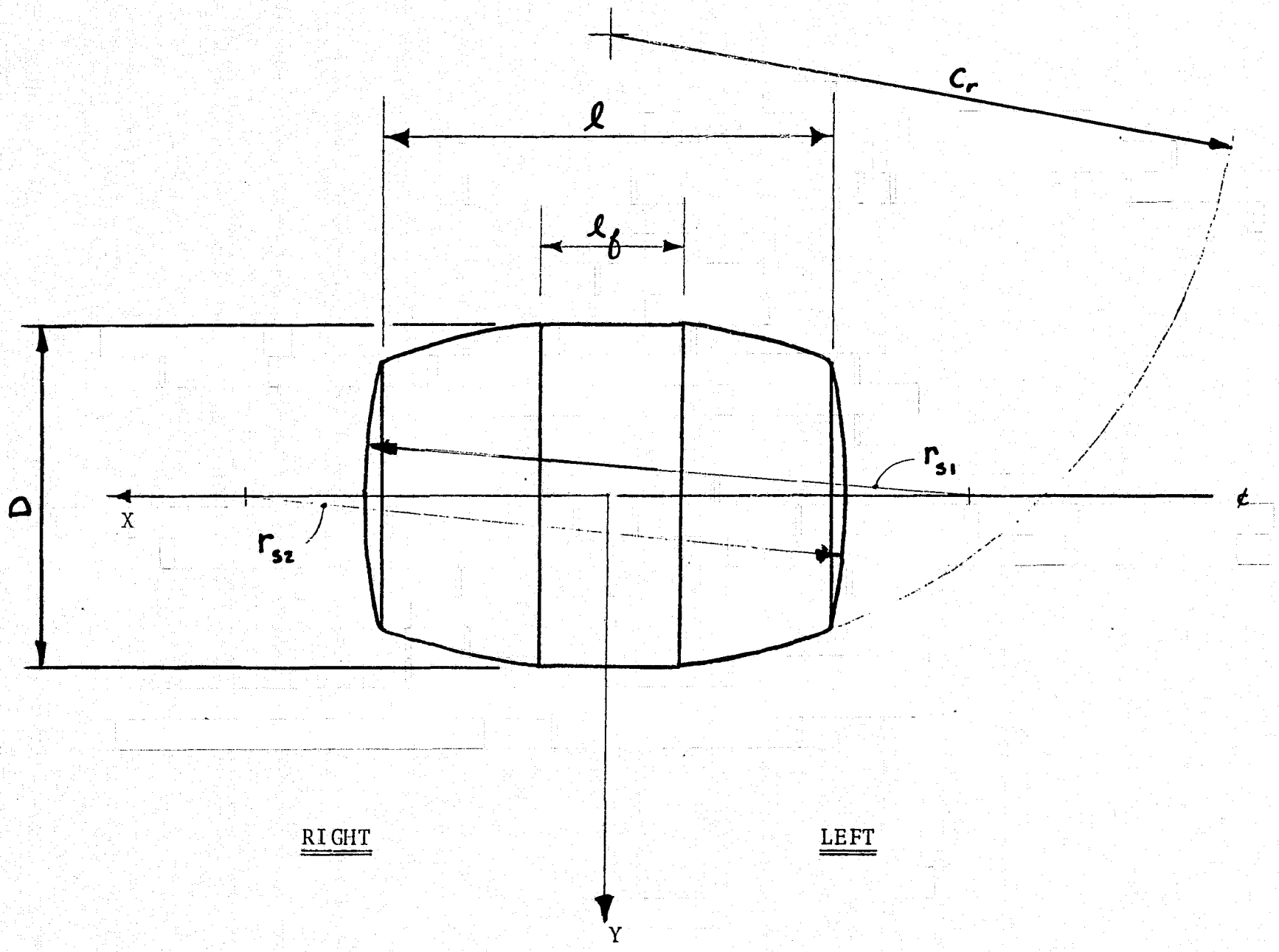

FIGURE C1: Roller Geometry Detail

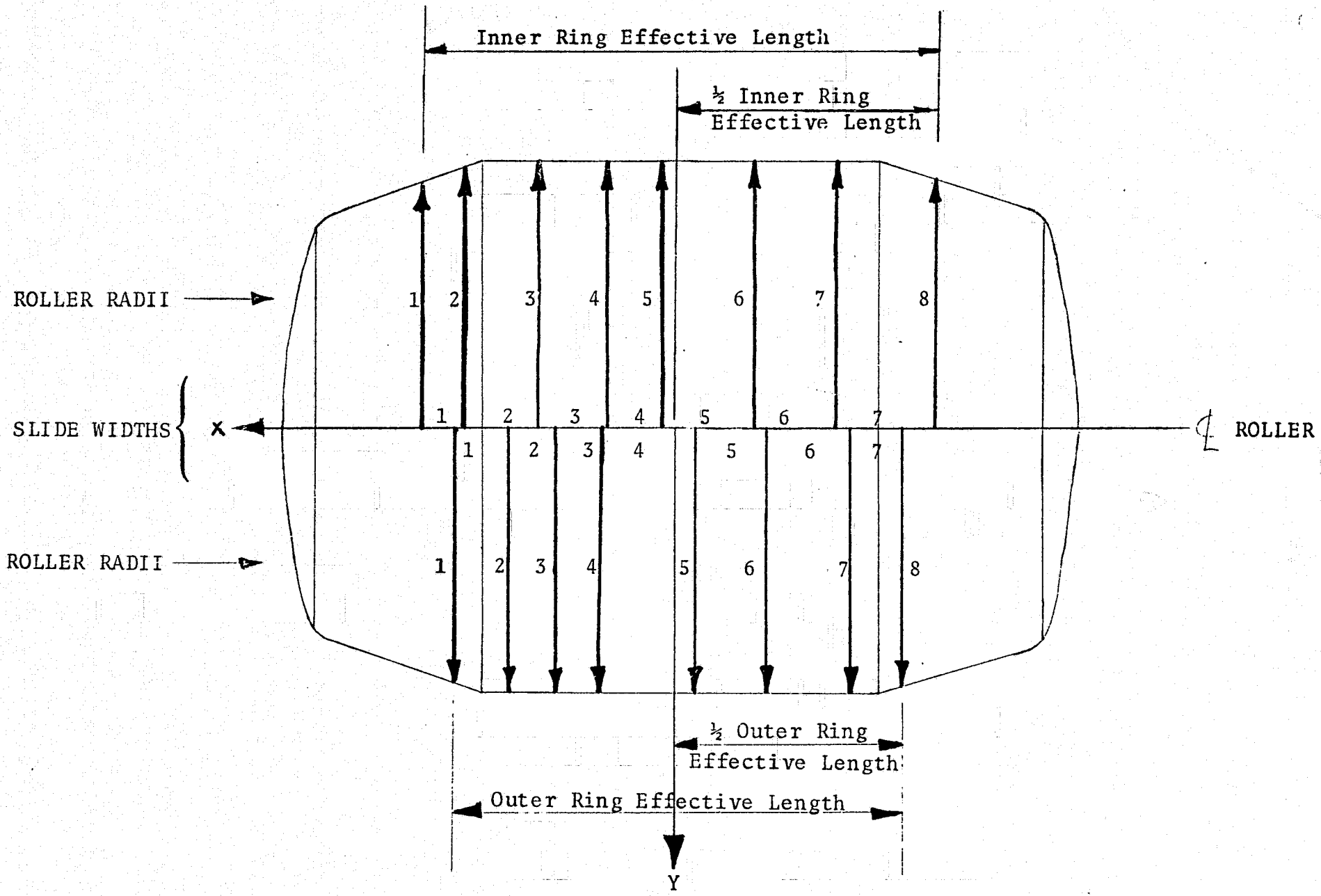

FIGURE 32: ROLLER SLICE GEOMETRY DETAIL.

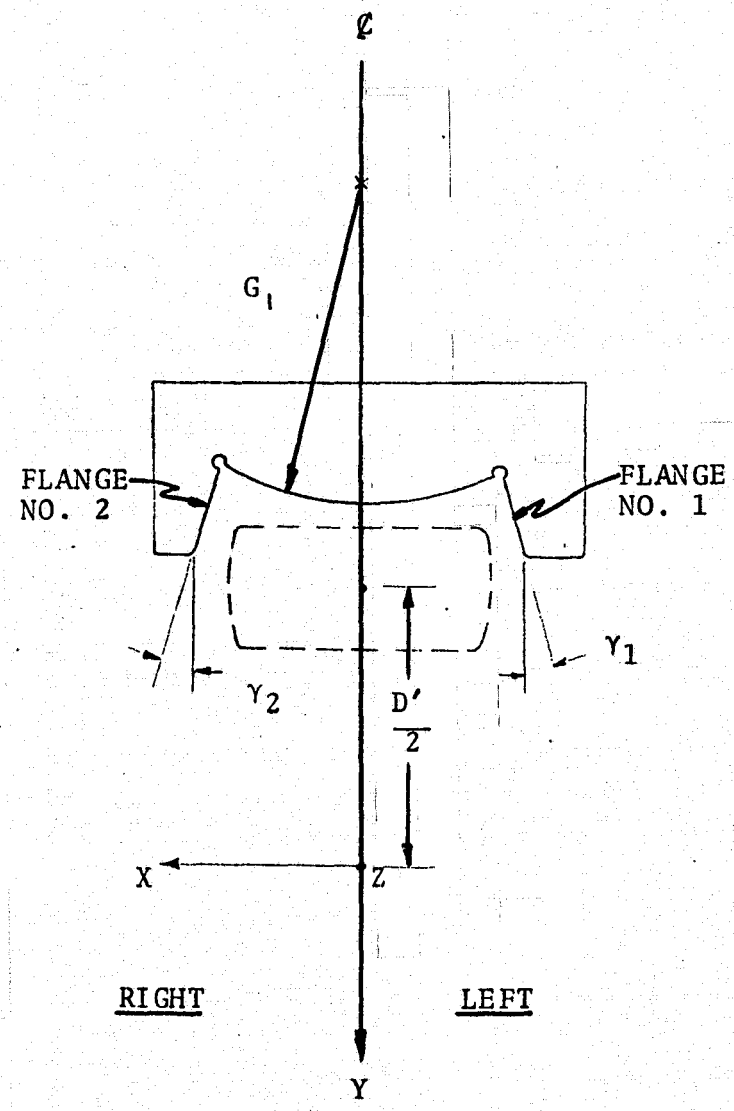

C3a) Outer Ring Data

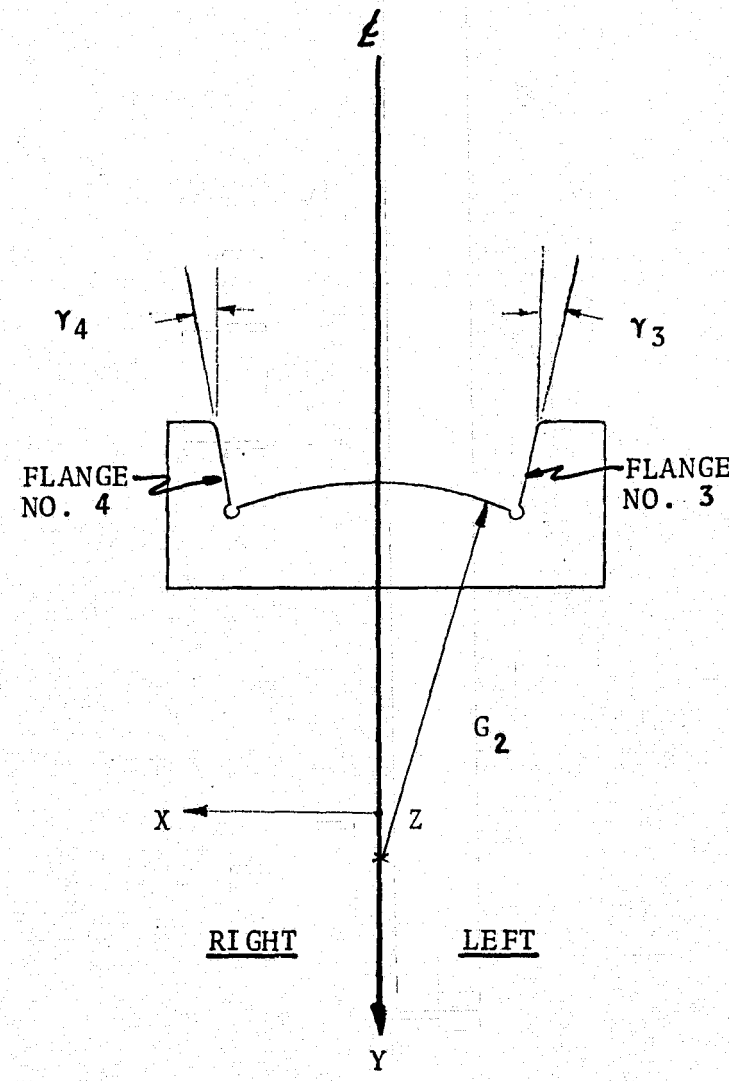

C3b) Inner Ring Data

FIGURE C3: RING GEOMETRY DETAIL

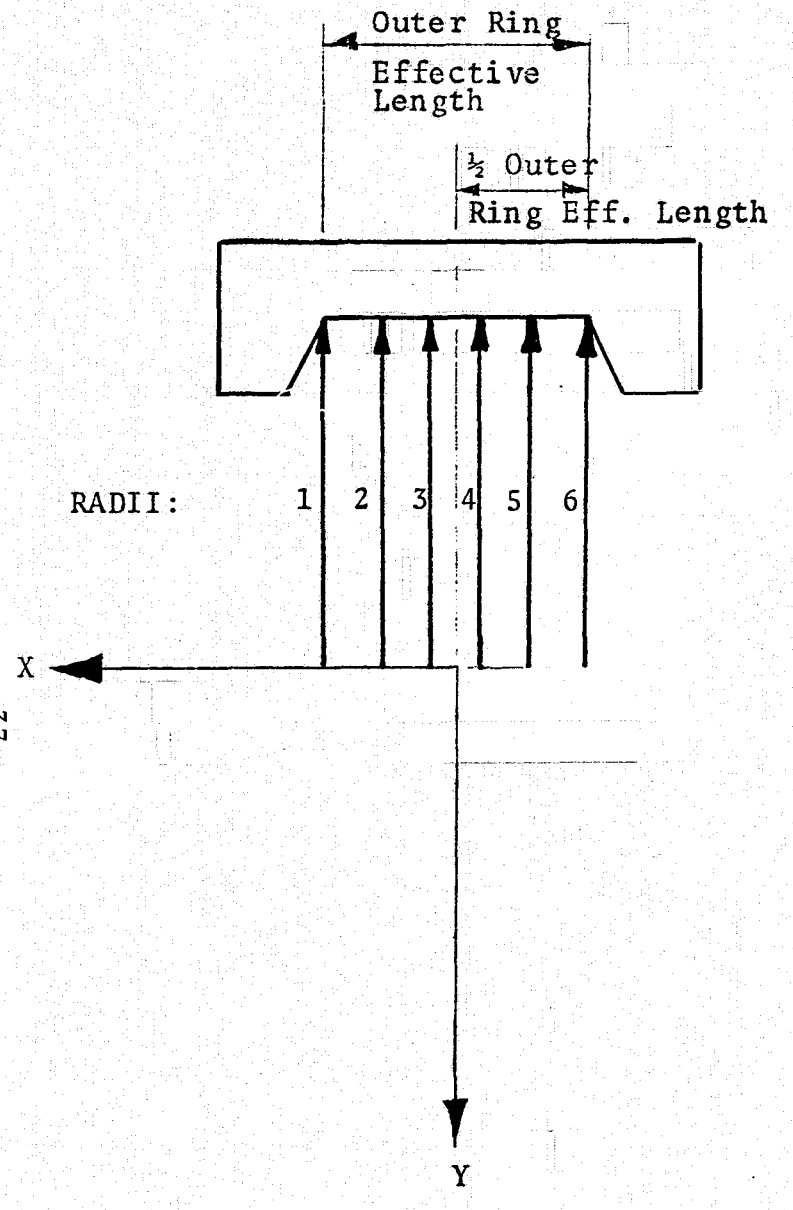

C4a) Outer Ring

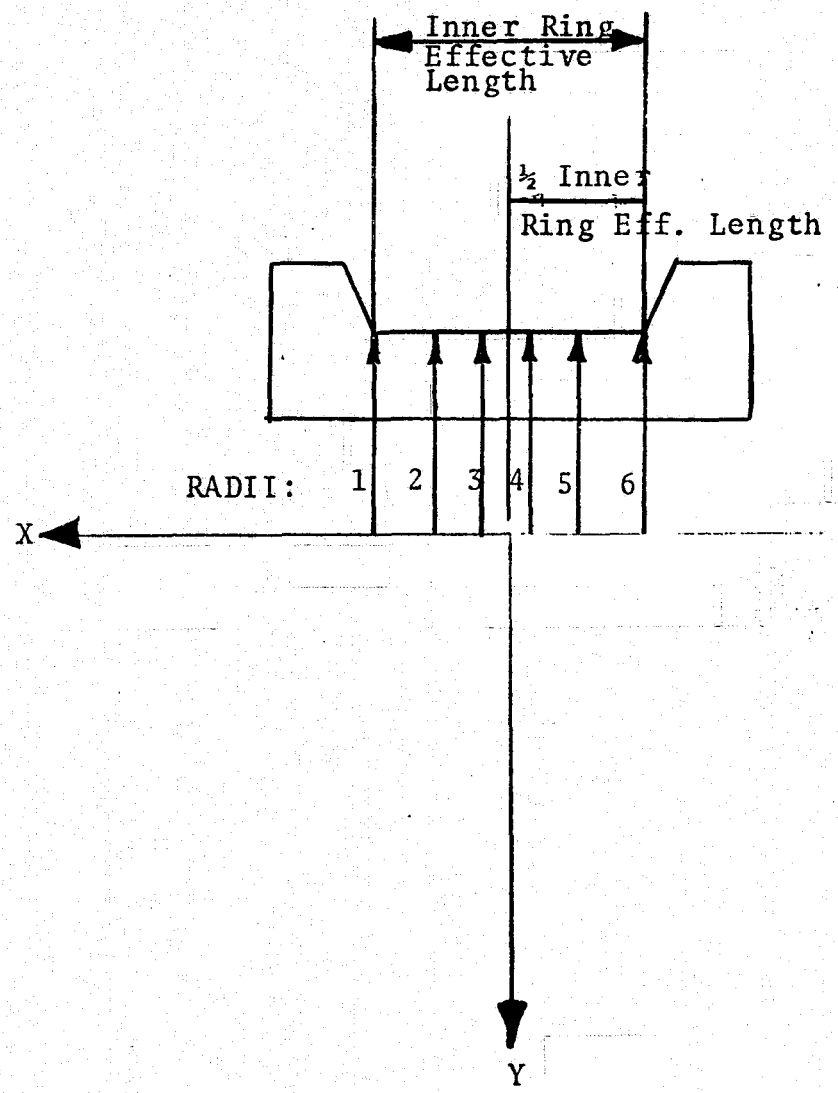

C4b) Inner Ring

FIGURE C4: RING SLICE GEOMETRY DETAIL

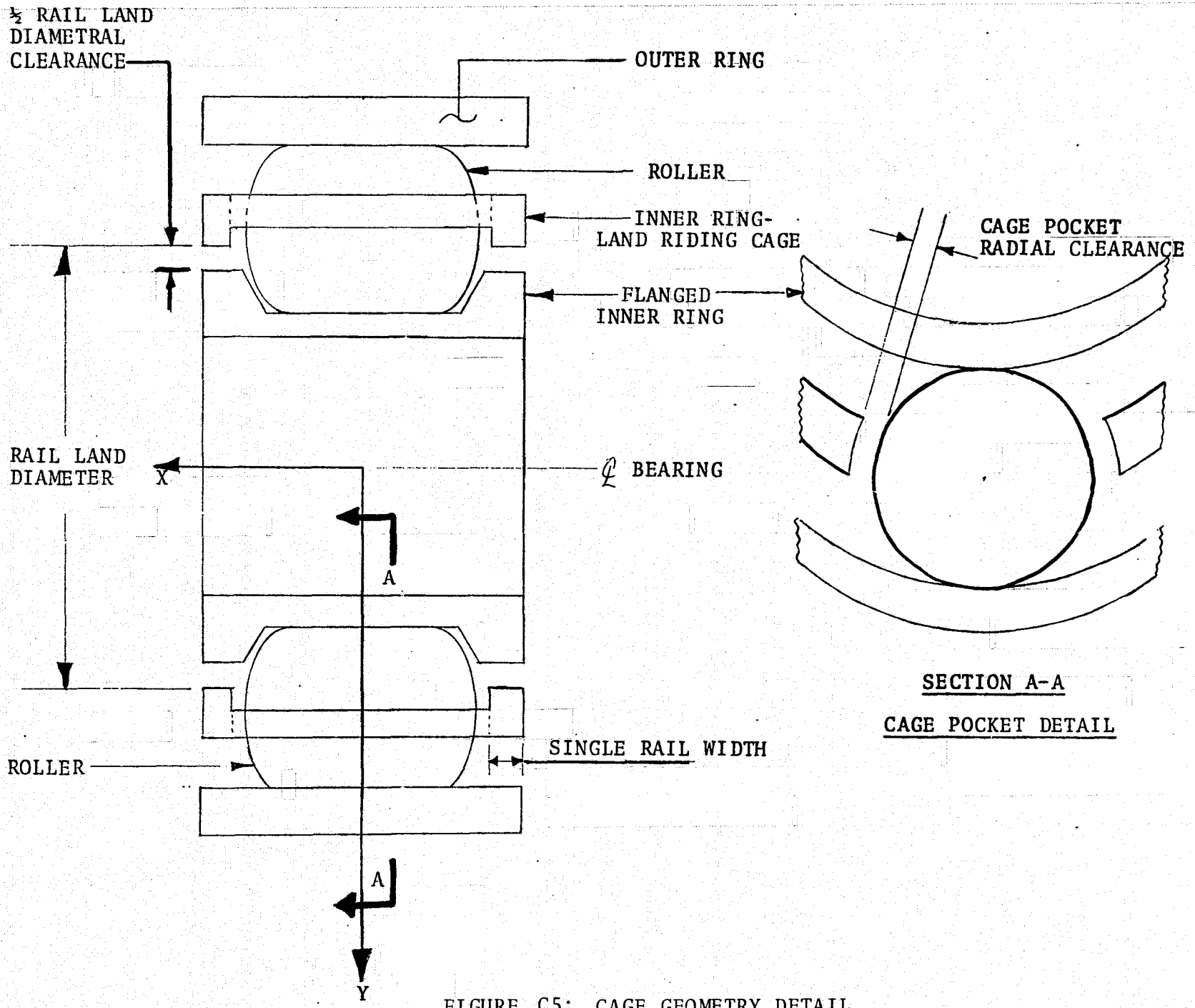

FIGURE C5: CAGE GEOMETRY DETAIL

APPENDIX D

LUBRICANT PROPERTY MODELS

VOLUME I

APPENDIX D: LUBRICANT PROPERTY MODELS

Calculations pertaining to friction on lubricant related processes require that the viscosity ν and the pressure-viscosity coefficient α be known as a function of temperature.

The kinematic viscosity ν (cs) at atmospheric pressure is calculated at a given temperature t (°F) from Walther's relation [3]

$$\log_{10} \log_{10} (\nu + 0.6) = A - B \log_{10} (t + 460) \qquad (1)$$

where A and B are constants determined by evaluating Eq. (1) at known values of $\nu = \nu(t)$.

Having calculated ν at a specific t, η is computed as

$$\eta = \nu\rho \qquad (2)$$

where ρ the lubricant density at temperature t given by:

$$\rho(t) = \rho(60°F) - G \{t-60°F\} \qquad (3)$$

Here, G is the lubricant coefficient of thermal expansion.

The pressure-viscosity index, α, is defined implicitly by the relation

$$\eta(p,t) = \eta_o e^{\alpha\rho} \qquad (4)$$

However, here α is calculated by a relation developed by Fresco [4]:

$$\alpha = (2.303)\ 10^{-4}\ [C+D\log_{10}\nu+ E(\log_{10}\nu)^2]^{\left(\frac{560}{t + 460}\right)} (in^2/lb) \qquad (5)$$

wherein ν is evaluated at temperature t (°F) and C, D and E are constants tabulated by Fresco.

Relevant lubricant properties for the oils whose properties have been programmed in CYBEAN are listed in Table D1.

TABLE D1

LUBRICANT PROPERTIES OF FOUR OILS

Oil No.	Oil Type	Kinematic Viscosity (cs) 100°F	210°F	Walther Equation Constants A	B	Density @ 60°F gm/cm³	Thermal Conductivity Kf Btu/Hr/Ft/°R	Thermal Coeff. of Expansion	Temp. Viscosity Coeff. ($°R^{-1}$)
1	Mineral Oil	64	8.0	10.349	3.673	0.8800	0.0671	3.52×10^{-4}	0.0193
2	MIL-L-7808G	12.8	3.2	10.215	3.698	0.9526	0.0879	3.94×10^{-4}	0.0132
3	C-Ether	25.4	4.13	11.452	4.113	1.201	0.0690	4.15×10^{-4}	0.0168
4	MIL-L-23699	28.0	5.1	10.207	3.655	1.010	0.0879	4.14×10^{-4}	0.0161

APPENDIX E

FORCES ACTING ON A ROLLING ELEMENT

VOLUME I

APPENDIX E: FORCES ACTING ON A ROLLING ELEMENT

Forces acting on a rolling element can be separated into those due to:

- Elastic Contact - generated at the outer and inner ring roller contacts and at the roller end - flange contact.
- Cage Interactions
- Hydrodynamic Friction - developed in the inlet region of the roller/race contact.
- Elastohydrodynamic - developed within the area of rolling-sliding contact of the roller/rings and roller/flanges.
- Centrifugal Effects
- Quasidynamic Effects and Element Drag

The following material develops relationships between forces, displacements and speeds for the roller loading described above.

1. Elastic Contact Forces

This section deals with the forces that develop as a result of the Hertzian elastic interaction between rollers and raceways and the roller end and flange.

1a. Roller Raceway Forces

Roller-raceway elastic forces are a function of the relative positions of the rollers and rings. When their displacements are specified, interpenetration magnitude is computed at various stations along the roller length at both the inner and outer rings. These stations are actually the disks which would result if the roller-raceway effective length were to be sliced by planes

parallel to their y-z planes. Slices are assumed to act independent of each other. The number of slices and geometry may either be calculated by the program or input as data by the user. (See Volume II and Appendices B and C of this volume.)

The relation between load and deformation for a line contact is given by [5].

$$Q = K_{\ell}\, \delta^{10/9}\, \ell_m^{8/9} \qquad (1)$$

Here, K_{ℓ} is a constant, δ is the elastic deformation and ℓ_m is the roller effective length. The k-th slice load at the m-th raceway is obtained from

$$Q_{k,m} = K_{\ell}\, \ell_m^{8/9}\, \delta_{k,m}^{10/9}\, \frac{W_k}{\ell_m} \qquad (2)$$

The elastic deformation for the k-th slice $\delta_{k,m}$, may be obtained by first computing the vector $\{\bar{B}_{km}\}_{\bar{R}}$, which connects the k-th roller slice center x-coordinate with the k-th ring slice center x-coordinate, Figures E-1 and E-2. The elastic deformation at the i-th rolling element location is then given by

$$\delta_{k1}^{i} = |\{\bar{B}_{k,1}^{i}\}_{\bar{R}}| + R_k - R_{k,1} + \Delta_o^i \qquad (3)$$

for the outer race contact, and by

$$\delta_{k2}^{i} = |\{\bar{B}_{k,2}^{i}\}_{\bar{R}}| - R_k - R_{k,2} + \Delta_I^i \qquad (4)$$

for the inner race contact. The terms Δ_o^i and Δ_I^i are included in Equations (3) and (4) to account for local displacements due to: deviation of the rings from a true circular profile and, deflection of the outer ring caused by interference fit pressure. Particular expressions for these effects are presented in Appendix F.

Equations (3) and (4) substituted in (2) enable the computation of the elastic load magnitude at the k-th slice as a function of the independent variables. Direction still must be established.

The unit vectors in the direction of resulting elastic force are assumed to act along the lines connecting interacting slice centers, i.e.:

$$\{\hat{u}^i_{km}\}_{\bar{R}} = C_m \left\{ \frac{\bar{B}^i_{k,m}}{|\bar{B}^i_{k,m}|} \right\}_{\bar{R}} \qquad (5)$$

where C_m is +1 when m=1 and C_m = -1 when m=2.

Equations (2) through (5) are used to give the resultant force vector acting on each slice of the i-th rolling element as

$$\{\bar{F}^i_{k,m}\}_{\bar{R}} = \frac{W_k K_\ell (\ell_m)^{8/9} (\delta^i_{k,m})^{10/9}}{\ell_m} C_m \left\{ \frac{\bar{B}^i_{k,m}}{|B^i_{k,m}|} \right\}_{\bar{R}} \qquad (6)$$

To obtain the vector in the roller frame whose terminus coordinates will be considered the theoretical point of contact, it is assumed that the point lies along the line connecting slice centers. The vector

$$\{\bar{P}^i_{k,m}\}_{\bar{R}} = \{ \bar{h}_k - (R_k - \delta^i_{k,m}) \hat{u}^i_{k,m} \}_{\bar{R}} \qquad (7)$$

locates the contact point, where $\{\bar{h}_k\}_{\bar{R}}$ is a vector whose terminus coordinates locate the k-th roller slice center, Figures E1 and E2.

Using (7) the moment vector generated by elastic contact forces is

$$\{\bar{M}^i_{k,m}\}_{\bar{R}} = \{\bar{P}^i_{k,m}\}_{\bar{R}} \times \{\bar{F}^i_{k,m}\}_{\bar{R}} \qquad (8)$$

1b. Roller End-Flange Contact

Figure E-3 shows a cross section through a cylindrical roller bearing having sphere-ended rollers and angled flanges. In this design, the flange surface is a portion of a circular cone whose axis is coincident with the ring x-axis, Figure E-4. The apex of the cone is located on the x-axis at C.

The flange surface is described by the equation of a right circular cone,

$$z = f(x,y) = [(x - c)^2 \cot^2\gamma_f - y^2]^{1/2} \qquad (9)$$

where γ_f is the flange angle, positive for circular cones that open in the positive x-direction.

If we assume the elastic contact force generated at the roller end flange contact to be normal to the flange surface, then its resultant must lie along the line normal to the surface $z=f(x,y)$ which passes through the theoretical point of contact $P(P_x, P_y, P_z)$. The equation of this line is given by

$$\frac{(x-P_x)}{\frac{\partial f}{\partial x}\Big|_{P_x,P_y}} = \frac{(y-P_y)}{\frac{\partial f}{\partial y}\Big|_{P_x,P_y}} = -(z - P_z) \qquad (10)$$

Introduce the vector $\{T\}_{\overline{R}}$ which locates the roller end sphere origin in the roller frame. We can transform the coordinates of this point into the flanged ring frame by using the general transform operators listed in Appendix B. We shall call the transformed vector $\{T\}_I$ and let its terminus point have the coordinates (T_x, T_y, T_z).

The roller end flange contact elastic force is also normal to the roller end surface and its resultant must pass through the sphere origin, (T_x, T_y, T_z). Using (T_x, T_y, T_z) in equations (9) and (10) we obtain

$$(T_x - P_x) = - \frac{(T_z - P_z)\ (P_x - C)\ \cot^2 \gamma_f}{[(P_x - C)^2\ \cot^2 \gamma_f - P_y^2]^{1/2}} \qquad (11)$$

$$(T_y - P_y) = \frac{(T_z - P_z)\ P_y}{[(P_x - C)^2\ \cot^2 \gamma_f - P_y^2]^{1/2}} \qquad (12)$$

$$P_z = [(P_x - C)^2\ \cot^2 \gamma_f - P_y^2]^{1/2} \qquad (13)$$

Equations (11) through (13) contain three unknowns (P_x, P_y, P_z) and are sufficient to determine the theoretical point of contact between the roller end and flange. However, by introducing a fourth equation and unknown, namely, the length of the line from points (T_x, T_y, T_z) to (P_x, P_y, P_z), we obtain the added benefit of closed form solution. The length of a line normal to the undistorted flange surface at the point (P_x, P_y, P_z), which joins this point with the sphere origin (T_x, T_y, T_z), is given by

$$D = [(T_x - P_x)^2 + (T_y - P_y)^2 + (T_z - P_z)^2]^{1/2} \qquad (14)$$

After algebraic reduction, the value D is obtained from the positive root of the quadratic equation

$$D = \frac{-S \pm (S^2 - 4RT)^{1/2}}{2R} \qquad (15)$$

where values for S, R and T are

$$R = \tan^2 \gamma_f - 1$$

$$S = \frac{2\sin^2 \gamma_f}{\cos \gamma_f} [(T_x - C) - \tan\gamma_f (T_y^2 + T_z^2)^{1/2}]$$

$$T = [(T_x - C) - \tan\gamma_f (T_y + T_z^2)^{1/2}]^2$$

The coordinates $P(P_x,P_y,P_z)$ are given by the following closed form functions of D:

$$P_x = T_y \tan\gamma_f [1 + (\frac{T_z}{T_y})^2]^{\frac{1}{2}} [1 - \frac{D\sin\gamma_f}{(T_y^2+T_z^2)^{\frac{1}{2}}}] + C \quad (16)$$

$$P_y = T_y [1 - \frac{D\sin \gamma_f}{(T_y^2+T_z^2)^{1/2}}] \quad (17)$$

$$P_z = T_z [1 - \frac{D\sin \gamma_f}{(T_y^2+T_z^2)^{1/2}}] \quad (18)$$

The resulting force acts along the line normal to the flange surface and passes through the sphere center. We may use equations (16) through (18) to define the unit vector in the direction of this force as

$$\{\hat{u}_e\}_{I(o)} = \left.\frac{\bar{d}_e^{\,i}}{|\bar{d}_e^{\,i}|}\right|_{I(o)} \quad (19)$$

where

$$\{\bar{d}^{\,i}\}_{I(o)} = \left.\begin{Bmatrix} (T_x - P_x)\hat{i} \\ (T_y - P_y)\hat{j} \\ (T_z - P_z)\hat{k} \end{Bmatrix}\right|_{I(o)} \quad (20)$$

These quantities are used to formulate the expression for the forces acting on the e-th flange from its elastic contact with the i-th rolling element,

$$\{\bar{f}_e^i\}_I = M' \left\{ \frac{\bar{d}_e^i}{|\bar{d}_e^i|} \right\}_I \tag{21}$$

where the computation of magnitude, M', is shown in Appendix H. The moment generated by this contact is given by

$$\{\bar{m}_e^i\}_I = \{\bar{p}_e^i\}_I \times \{\bar{f}_e^i\}_I \tag{22}$$

where

$$\{\bar{p}_e^i\}_I = \begin{Bmatrix} P_x \hat{i} \\ P_y \hat{j} \\ P_z \hat{k} \end{Bmatrix}_I \tag{23}$$

2. Cage Analysis

Several authors [6,7,8] have shown, by experiment and analysis, that the cage imposes a substantial effect upon rolling element kinematics. Its presence within the bearing complement can be especially influential when the bearing is operated under light radial load and high speed. Under such conditions cylindrical roller bearings can sustain severe skidding at the inner raceway contacts. Bearing speeds at any instant in time are no longer fully determined by the raceway contact forces alone.

The typical high speed cylindrical roller bearing cage is manufactured so that it is supported within the assembly by guide rings on its outboard sides. The cage guide rings interact with shoulders manufactured on either the outer or inner rings.

The inner ring guide design is prevalent, since the torque induced at the guide ring/shoulder interaction tends to be in the direction of roller motion and helps in the reduction of skidding.

The clearance between the guide rails and the ring shoulder is sufficient to permit limited extent but full six degree of freedom cage motion. However, for current practical considerations. the cage motion can be considered to reside in a plane normal to the bearing axis. This planar motion is encouraged by the rotation induced gyroscopic counter moments which tend to keep the cage rotation about a single axis.

To analyze the configuration, a coordinate frame $(x,y,z)_c$ is attached to the cage and defined to be coincident with the respective ring coordinate frame when the cage is centered on the guide shoulders.

The lubricant forces which develop at the guide ring when the cage center is displaced radially to the point y', z' in the y_c-z_c plane can be conveniently computed from the hydrodynamic solution for short, self-acting journal bearings [9]:

$$W'_y = \pm \frac{\eta_o U L^3}{C^2} \frac{\varepsilon^2}{(1-\varepsilon^2)^2} \tag{24}$$

$$W'_z = + \frac{\eta_o U L^3}{C^2} \frac{\pi\varepsilon}{4(1-\varepsilon^2)^{3/2}} \tag{25}$$

The upper sign is used for inner ring shoulder guided cages and the lower sign for the corresponding outer ring condition. The value ε is related to the displacement by

$$\varepsilon = (y'^2 + z'^2)^{1/2}/C \tag{26}$$

The torque induced on the cage in the presence of lubrication is

$$M^* = \pm \frac{\eta_o \bar{V} R^2 L}{C} \frac{2\pi}{(1-\varepsilon^2)^{1/2}} \qquad (27)$$

The forces W'_y and W'_z act at the point of closest approach between the cage guide rail and support shoulder.

We introduce the azimuthal angle ψ', which locates the point of closest approach and is measured CCW positive from the cage y_c-axis. The forces acting on the cage from its interaction with the pilot surface may then be brought into the cage reference frame by performing the transformation

$$\begin{bmatrix} M_x \\ W_y \\ W_z \end{bmatrix} = \begin{bmatrix} 1 & 0 & 0 \\ 0 & \cos\psi' & -\sin\psi' \\ 0 & \sin\psi' & \cos\psi' \end{bmatrix} \cdot \begin{bmatrix} M^* \\ W'_y \\ W'_z \end{bmatrix} \qquad (28)$$

The forces which develop within the boundaries of the cage pocket are induced by the interaction of the roller with the leading and trailing pocket webs and the pocket sides. Magnitudes of these forces depend upon the characteristics of the interacting geometries.

Several pocket designs are currently manufactured for use in high speed cylindrical roller bearings. Differences reside in the use of materials and the degree of web conformity to roller shape.

Several computation procedures, and thus several opportunities, exist for the calculation of roller-web interaction forces. In the current analysis, the web geometry is simplified to that of a rectangular cavity, and the roller to that of a cylinder. End effects, such as those which would appear as a result of the roller interacting with the cage pocket sides, are neglected.

The web forces can be considered to be a function of roller rotational speed and the relative position of the roller within the cage pocket. Assuming that the rolling element orbital velocity remains constant as it traverses the distance corresponding to one half the pitch spacing on either side of its nominal azimuth position, the value of the roller center cage pocket center offset for the i-th rolling element (Z_i) can be computed from knowledge of the orbital speeds as follows:

$$Z_i = \frac{\pi d}{n_r} \left(\sum_{j=2}^{i} \left[\frac{(w_o)_{j-1} + (w_o)_j}{2W_c} - 1 \right] \right) - Z_1 + y'_c \sin\psi_i - Z'_c \cos\psi_i \qquad (29)$$

$$i = 2, 3, \ldots n_r$$

where Z_1 is the initial circumferential offset and W_c is the cage rotational speed, assumed to be the average of the roller orbital speeds.

The means for calculating the cage web force evolves from the assumption that the pocket load is borne hydrodynamically by a lubricant film existing in the gap between the roller surface and web.

The equation relating the film thickness to load magnitude is of the form

$$F = K'/h_o \qquad (30)$$

where K' is a constant and h_o is the hydrodynamic film thickness. In the context of the current numerical analysis, field equations containing relationships of this form are extremely difficult to solve due to the coupling with many of the independent variables.

A force-displacement relationship of the form

$$F_i = -K Z_i \qquad (31)$$

has currently been chosen. Here, the value of K is selected so that equations (31) and (30) are equal at F = 66N (15 lb). The latter value is chosen to represent practical upper limits for web loading values. Note that the direction of F_i is opposite to Z_i.

The radially directed friction force is assumed to be of the form

$$f_i = \mu_h F_i \tag{32}$$

where μ_h is a hydrodynamic friction coefficient and may be computed from established equations describing the lubrication of a rigid cylinder near a plane [10]. The moment about the x-axis is given by

$$M_{w_i} = \frac{d}{2} \mu_h |F_i| \tag{33}$$

In vector format, the i-th rolling element loading due to cage interaction is

$$\{\overline{F}_c{}^i\}_{\overline{R}} = \begin{Bmatrix} 0 & \hat{i} \\ f_i & \hat{j} \\ F_i & \hat{k} \end{Bmatrix}_{\overline{R}} \tag{34}$$

$$\{\overline{M}_c{}^i\}_{\overline{R}} = \begin{Bmatrix} M_{w_i} & \hat{i} \\ 0 & \hat{j} \\ 0 & \hat{k} \end{Bmatrix}_{\overline{R}} \tag{35}$$

3. Inlet Region Hydrodynamic Friction Forces

During high speed lubricated operation, the roller-race and roller end-flange contacting surfaces are separated by a fluid film. The formation of this film depends largely on the ability of the contacting bodies to pump lubricant into the high pressure region of the contact.

The fluid immediately preceding the contact, commonly referred to as a meniscus, forms a reservoir from which lubricant is fed. The lubricant is pumped into the high pressure area by the shearing action created by the rolling/sliding motion of the contacting bodies. The non-uniform pressure distribution created on the reservoir fluid contributes to rolling resistance.

Expressions for these forces have been developed for point (ellipsoidal) contacts [11,12], as well as for line contacts [13].

The hydrodynamic forces F_r, F_s and F_n are displayed in Figure E5. The special case of contact between two disks is illustrated.

The force F_r acts in the same direction on both contacting bodies and opposite to the direction of motion. F_s acts in opposite directions on the two bodies in such a way as to tend to increase the speed of the slower body and decrease the speed of the faster body.

The forces F_1 and F_2 are the integrals of the hydrodynamic pressure distribution in the inlet and act through the centers of the two bodies. The component of these forces in the y direction represents the (small) portion of the total load supported hydrodynamically. The components F_{n1} and F_{n2} acting in the x-direction contribute to the force balance in the rolling direction.

The magnitudes of F_r, F_s and F_n have been obtained in the literature [13]. Normal friction forces acting through the centers of the two cylinders of radii R_{y1} and R_{y2} and of length ℓ are:

$$\begin{bmatrix} F_{n1} \\ F_{n2} \end{bmatrix} = \begin{bmatrix} R_{y2} \\ R_{y1} \end{bmatrix} \ell \, \bar{P}_{xo} \, (2\eta R^{1/2}) \, [h^{1/2} (R_{y1}+R_{y2})]^{-1} \, \tilde{u}$$

Pumping forces are

$$F_r = 0.5 \, (F_{n1} + F_{n2})$$

Sliding friction has been determined to be

$$\begin{bmatrix} F_s(\text{outer ring}) \\ F_s(\text{inner ring}) \end{bmatrix} = B \begin{bmatrix} V \, (\text{outer}_{\text{inner}}) \\ u \, (\text{outer}_{\text{inner}}) \end{bmatrix} \cdot \frac{R}{2\alpha} \left[\frac{2\eta u \, (\text{outer}_{\text{inner}}) \alpha}{R_x} \right]^{2/3}$$

where u = entrainment velocity = $(u_2 + u_1)/2$ and V = sliding velocity = $u_2 - u_1$

and the dimensionless coefficient $\bar{P}_{xo}$ is given in reference [13].

Retaining vector format, the net force acting on the i-th rolling element due to hydrodynamic friction is given by

$$\{\bar{H}^i\}_{\bar{R}} = \begin{Bmatrix} (F_s + F_n)_x \hat{i} \\ (F_s + F_n)_y \hat{j} \\ (F_s + F_n)_z \hat{k} \end{Bmatrix}_{\bar{R}} \tag{36}$$

and the net moment acting on the i-th rolling element due to hydrodynamic friction is given by

$$\{\bar{G}^i\}_{\bar{R}} = \begin{Bmatrix} (F_r + F_s)(R_{y1})_x \hat{i} \\ (F_r + F_s)(R_{y1})_y \hat{j} \\ (F_r + F_s)(R_{y1})_z \hat{k} \end{Bmatrix}_{\bar{R}} \tag{37}$$

4. Elastohydrodynamic Forces

The calculation of forces which develop within the area of the concentrated contact follows.

Pure rolling motion does not exist between the roller and raceways. Interacting geometries and elastic contact deformation prohibit this. As a result, various points within the contact boundaries experience different degrees of sliding. This sliding gives rise to fluid shear and asperity interactions, which in turn produce forces in the contact area.

Several authors have addressed this problem during the past decade, and produced important empirical and semi-empirical models which relate the magnitude of force to measurable variables.

The model employed in the current effort was developed by Allen, et al [14].

The traction force is calculated by integrating the fluid shear over the entire contact area. Allen assumes the fluid shear to behave exponentially with pressure until some critical contact pressure is achieved, usually 6.89 N/MM (1,000 psi), above which point the shear can become a constant fraction of the normal pressure. This relationship is stated by

$$\tau = \eta_o e^{\alpha p} \{\bar{s}\} h^{-1} \quad \text{when } \tau < \tau_c \tag{38}$$

or

$$\tau = \bar{f}p \quad \text{when } \eta_o e^{\alpha p} \{\bar{s}\} h^{-1} > \bar{f}p \text{ and } > \tau_c \tag{39}$$

where h is the elastohydrodynamic film thickness, computed by the Loewenthal model [15].

Roller raceway contact friction is obtained as the sum of the friction forces evaluated at each elemental slice area. For a typical slice interaction this is expressed as

$$T = 2\eta_o b \{\bar{s}\} \int_0^b e^{\alpha \bar{p}} [1-(\frac{z}{b})^2] \cdot h^{-1} \, dz \qquad (40)$$

where $\bar{p}$ is the maximum Hertzian contact pressure, b the contact half width and z a dummy coordinate measured from the center of the contact (z = 0) outward. Note that sliding is assumed constant across the slice contact area and is computed by simply taking the difference between the surface velocities of mating slices at the theoretical point of contact (see equation 7):

$$\{\bar{s}^i_{km}\} = \{\bar{w}_m\}_{\bar{R}} \times \{\bar{P}^i_{km}\}_{\bar{R}} - \{\bar{w}_o{}^i\}_{\bar{R}} \times \{\bar{P}^i_{km}\}_{\bar{R}} - \{\bar{w}^i_r\}_{\bar{R}} \times \{\bar{P}^i_{km}\}_{\bar{R}} \qquad (41)$$

Hence, the k-th slice traction force is denoted by $\{\bar{T}^i_{km}\}_{\bar{R}}$.

If it is assumed that the resultant slice traction force acts through the theoretical contact point, the net moment produced is given by

$$\{U^i_{km}\} = \{\bar{P}^i_{km}\} \times \{\bar{T}^i_{km}\}_{\bar{R}} \qquad (42)$$

The roller end-flange contact is treated in a similar fashion, although in this instance the simplifying assumptions of uniform sliding/uniform pressure over the contact area is invoked, yielding

$$\{\bar{t}^i_e\}_{I(o)} = \{\bar{s}^i_e\}_{I(o)} \quad \tau^i_e \, A^i_e \qquad (43)$$

Here, A_e^i is the contact area of the e-th flange contact for the i-th rolling element. Sliding velocity is defined as the difference between the flange surface velocity and roller end surface velocity at the contact point (see equation 23):

$$\{\bar{s}_e^i\}_I = \left\{\{\bar{w}_r^i\}_{\bar{R}} \times \{\bar{P}_e^i\}_{\bar{R}}\right\}_I + \{\bar{w}_o^i\}_I \times \{\bar{P}_e^i\}_I - \{\bar{w}_m^i\}_I \times \{\bar{P}_e^i\}_I \quad (44)$$

Finally, the moment produced at the roller end flange contact is obtained from equation (23) as

$$\{\bar{u}_e^i\}_{I(o)} = \{\bar{P}_e^i\}_I \times \{\bar{t}_e^i\}_{I(o)} \quad (45)$$

5. Other Forces

Rolling Element Drag

After accounting for all rolling element contact friction forces, there is a residual drag acting on the rolling element. This force arises as a result of the rolling element plowing through the air-oil mixture in the bearing cavity. To evaluate this force we employ a model of the following form:

$$\{F_{DRAG}^i\}_{\bar{R}} = -\left\{\left[\frac{\rho A C_v d^2}{8\,g}(w_o^i)^2\right]\hat{k}\right\}_{\bar{R}} \quad (46)$$

where C_v is a drag coefficient given in [16]. The density of the air-oil mixture in the bearing cavity, ρ, is given by

$$\rho = \rho_o \bar{x} \quad (47)$$

where $\bar{x}$ is the fractional amount of lubricant in the bearing cavity and ρ_o is the lubricant density.

Quasidynamic Forces

Equivalent inertial forces and moments are introduced to apply the equations of static equilibrium when acceleration is present. Using Newton's second law of motion for a single mass, Kellstrom [17] derived expressions for these forces and moments. They are:

$$\{\bar{F}_q^i\}_{\bar{R}} = -\frac{d}{2}\, m \begin{Bmatrix} 0 & \hat{i} \\ (w_o^i)^2 & \hat{j} \\ (w_o^i)^2 \frac{dw_o^i}{d\psi} & \hat{k} \end{Bmatrix}_{\bar{R}} \qquad (48)$$

and

$$\{\bar{M}_q^i\}_{\bar{R}} = \frac{(w_o^i)\, m\, D^2}{g} \left(\frac{dw_r^i}{d\psi}\right) \hat{i} \qquad (49)$$

Note that terms containing $m\ddot{x}$, $m\ddot{y}$, $\dot{\gamma}_s$ and $\dot{x}$ are neglected.

Derivatives are approximated from values of speed for adjacent elements.

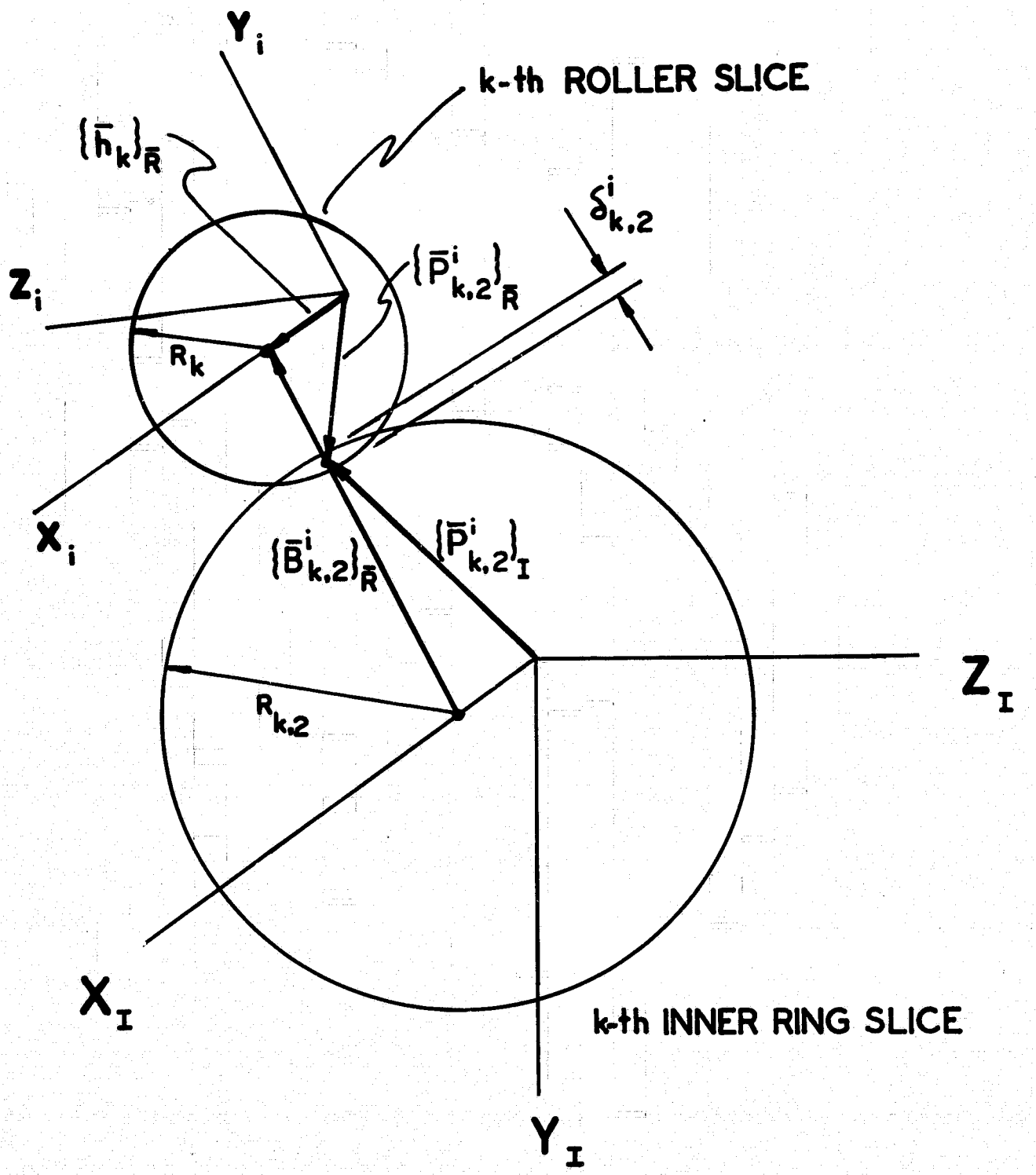

FIGURE E-1: INNER RING AND ROLLER SLICE INTERACTION DETAIL.

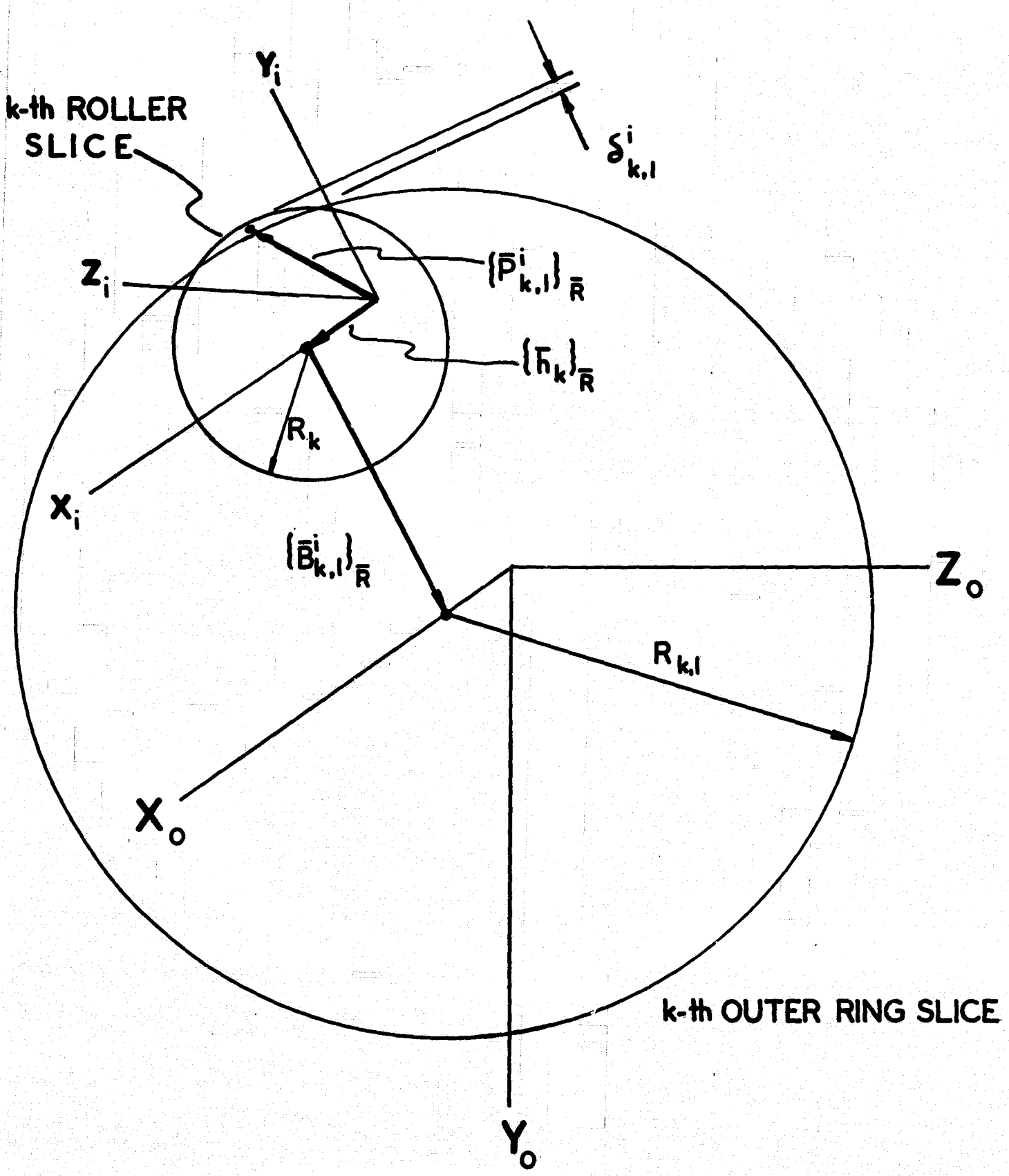

FIGURE E-2: OUTER RING AND ROLLER SLICE INTERACTION DETAIL

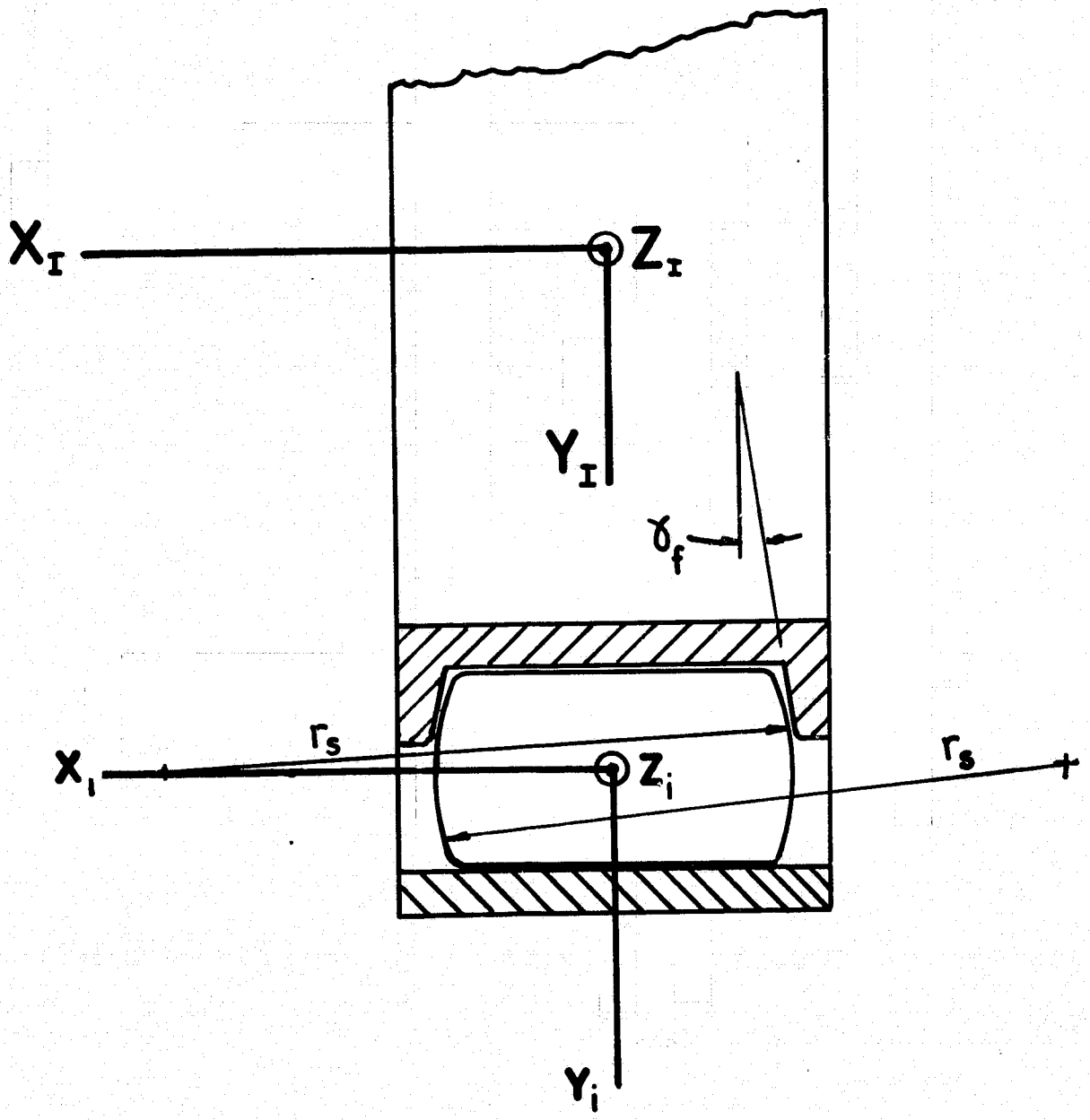

FIGURE E-3:CROSS SECTION THROUGH A CYLINDRICAL ROLLER BEARING HAVING A FLANGED INNER RING.

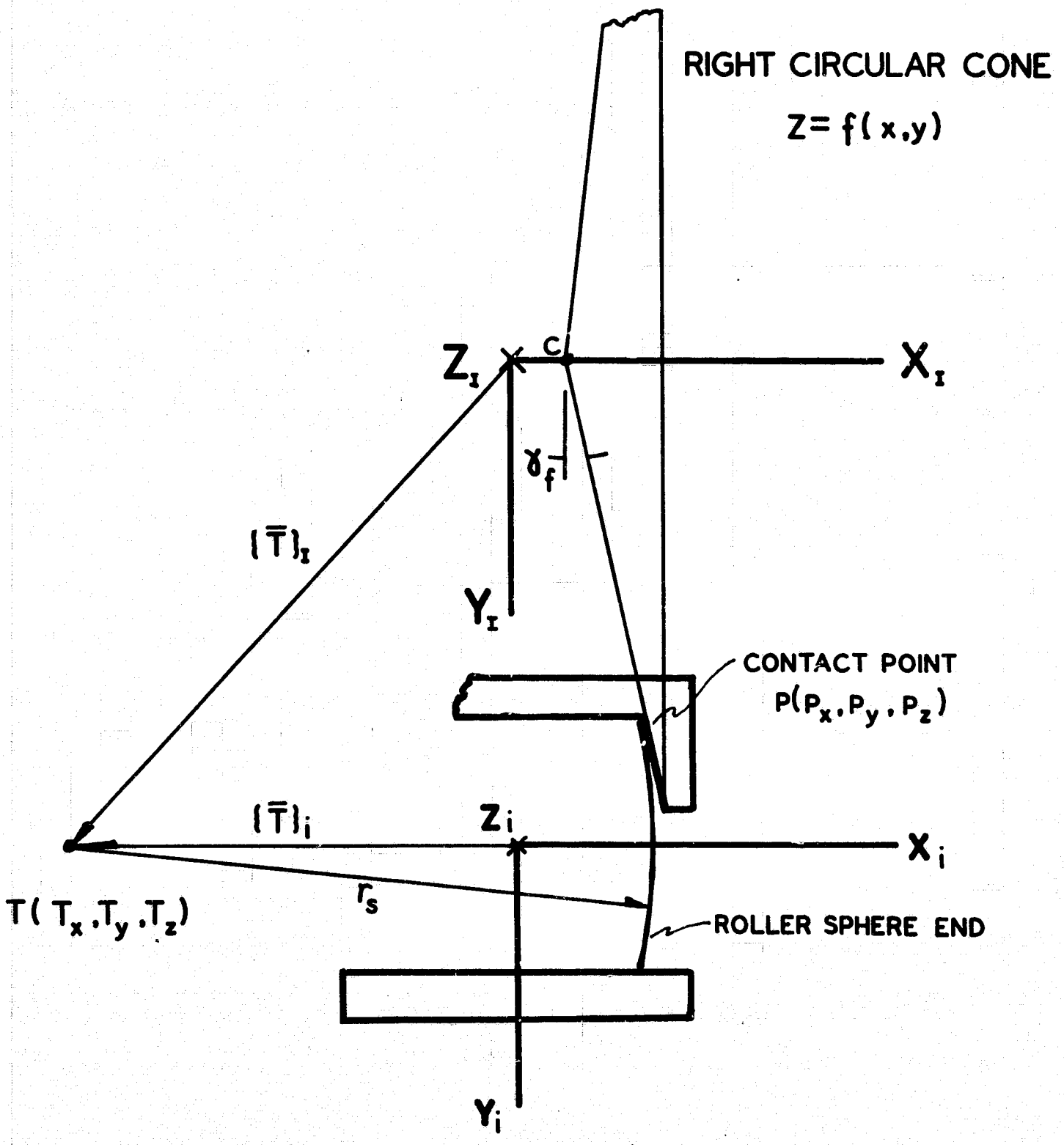

FIGURE E-4: ROLLER END-FLANGE CONTACT GEOMETRY

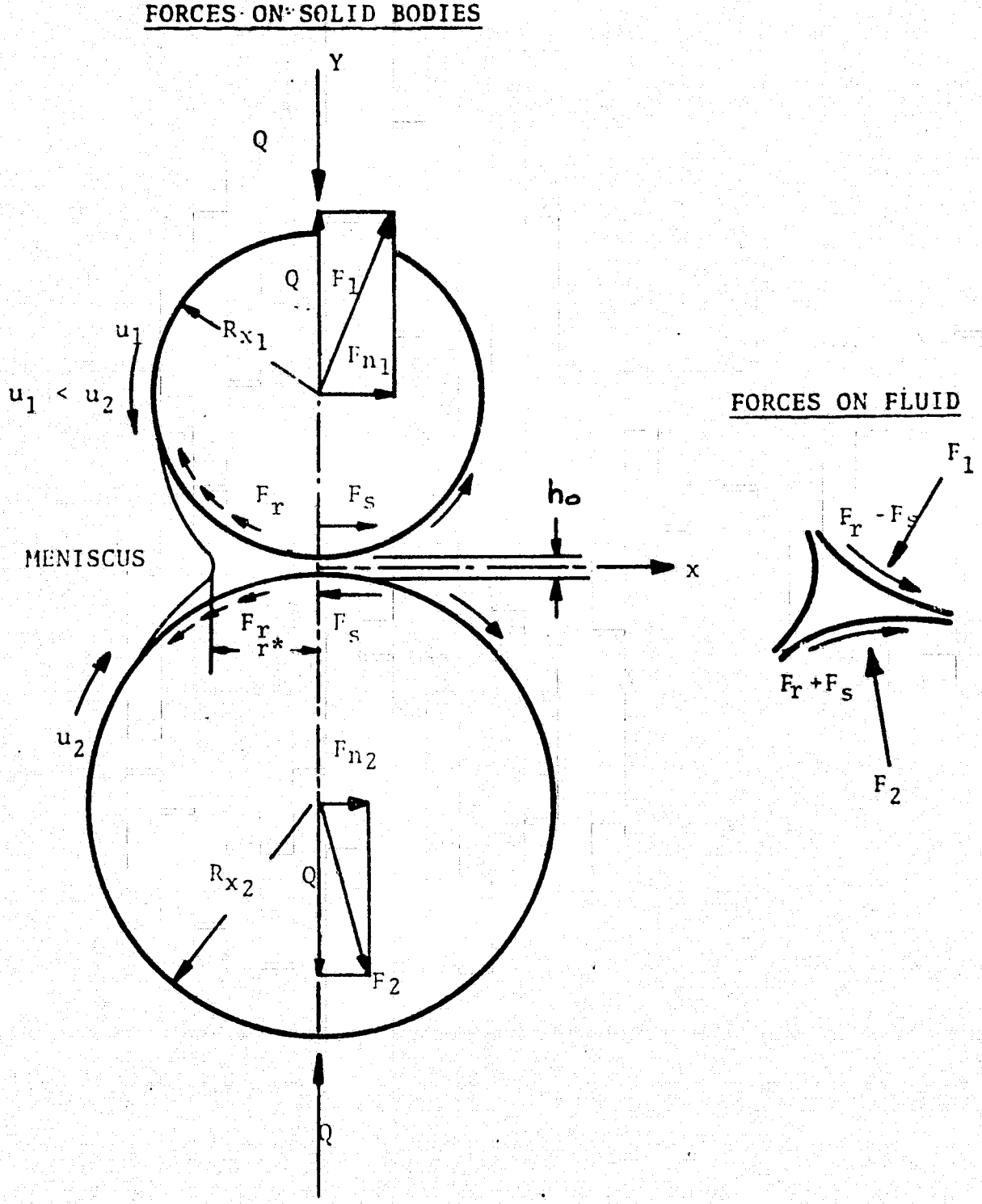

FIGURE E-5:HYDRODYNAMIC FRICTION FORCES ON SLIDING DISKS.

NOMENCLATURE

Appendix E

A	frontal area of a rolling element (in^2)
C	cage land radial clearance (in)
C_r	cage pocket radial clearance (in)
D	roller diameter (in)
E	modulus of elasticity (PSI)
I	effective cross section moment of inertia (in^4)
L	cage land width (in)
K_ℓ	load deformation constant for a line contact
K_p	load deformation constant for a point contact
R	$(1/R_{y1} + 1/R_{y2})^{-1}$ (in)
R_c	cage land radius (in)
R_k	radius of the k-th roller slice (in)
$R_{k,m}$	radius of the k-th raceway slice of the m-th raceway (in)
U	entrainment velocity (in/sec)
V	net sliding (in/sec)
W	slice width (in)
b	contact half width (in)
d	pitch diameter (in)
g	gravity constant
h	film thickness (in)
ℓ_m	roller raceway effective length at the m-th raceway (in)

m	roller mass (lb-sec /in)
n	number of roller-raceway slices
n_r	number of rollers
r_s	roller end sphere radius (in)
u	surface velocity (in/sec)
w_m	rotational speed of the m-th raceway (rad/sec)
w_o^i	orbital speed of the i-th roller (rad/sec)
w_r^i	rotational speed of the i-th roller (rad/sec)
ψ_i	azimuth angle locating the i-th rolling element, measured CCW positive from the y-axis in the y-z plane of the outer ring frame
γ_f	flange angle (rad)
γ_y	roller skew (rad)
γ_z	roller tilt (rad)
η_o	absolute viscosity (lb-sec/in)
$\{\overline{V}\}_\alpha$	a vector in the α coordinate system
$\{\hat{V}\}_\alpha$	a unit vector in the α coordinate system
$\lvert\{\overline{V}\}_\alpha\rvert$	magnitude of the vector $\overline{V}$
$\hat{i},\hat{j},\hat{k}$	unit vectors in the x, y and z directions, respectively

Program input and output are in SI units although calculations are performed in English units.

Subscripts

e	refers to the e-th flange
i	refers to the i-th roller in complement
k	refers to the k-th slice
ℓ	refers to the ℓ-th rolling element outer ring contact load
m	refers to the m-th raceway, i.e., m=1 for the outer race, m=2 for the inner

Notation

X	vector cross product

APPENDIX F

FITTING OF NON-CIRCULAR RINGS INTO NON-CIRCULAR HOUSINGS

VOLUME I
APPENDIX F: FITTING OF NON-CIRCULAR RINGS INTO NON-CIRCULAR HOUSINGS

Several authors have shown that the flexural stiffness of the outer and inner rings imposes a first order effect on the rolling element load distribution, and hence on the bearing performance. However, these investigations have been limited to the analysis of bearings for which the reactive housing/ring load distribution has been assumed. In the current analysis the reactive load distribution and hence the deformed shapes of both the housing and outer ring are left as variables to be defined by solution.

The rolling element load at the outer ring is substantially higher than that present at the inner ring for high speed bearing applications. This is due to roller forces generated by centrifugal effects. High speed cylindrical roller bearings in particular, are typically operated under light imposed radial loads. Thus, for the present analysis, the deformation of the composite outer ring/housing is detailed and the inner ring is assumed to be a flexurally rigid elastic solid.

To induce roller preload, many cylindrical roller bearings are manufactured with a non-circular outer ring surface. The radius of the outer profile of such a ring is a function of azimuthal position, i.e.:

$$r_I(\theta) = R_I \left(1 + e_I \cos n_I \left(\theta - \Phi_I\right)\right) \qquad (1)$$

Additionally, the housing itself may also be manufactured in a similar manner so that:

$$r_o(\theta) = R_o \left(1 + e_o \cos n_o \left(\theta - \Phi_o\right)\right) \qquad (2)$$

Here, R_o and R_I are the average radii of the housing and ring, e_o and e_I the non-circular semi-amplitude (expressed as a fraction of the average radius), Φ_o and Φ_I are phase angles and n_o and n_I the number of lobes (Figure F-1).

The deformed shape that the outer ring assumes is governed by the free shapes of the ring and housing, the rolling element loads and the reaction pressure distribution at the housing/ring interface.

Currently, no closed form solution exists for the deformation of thin circular rings loaded by an arbitrary pressure distribution. However, expressions have been derived for the deformation of a ring under the influence of discrete point radial loads. These solutions may be used to construct an equivalent load distribution on a given ring. The deflection of a particular point subject to an arbitrary load distribution is then defined by the superposition of the deflections obtained from each point load in the distribution.

Additionally, from equilibrium considerations, we require that the sum of the reaction loads has to equal the sum of the roller applied loads:

$$\sum_{i=1}^{m} F_i \cos\phi_i = \sum_{j=1}^{n} G_j \cos\gamma_j \qquad (3)$$

$$\sum_{i=1}^{m} F_i \sin\phi_i = \sum_{j=1}^{n} G_j \sin\gamma_j \qquad (4)$$

Where F_i, i=1, m are the roller loads and G_j, j=1, n are the point loads which approximate the reaction pressure distribution.

The deflection of the ring from both the roller and reaction loads can be computed from:

$$D_I(\Theta) = \sum_{i=1}^{m} F_i C_I(\beta-\phi_i) - \sum_{j=1}^{n} G_j C_I(\beta-\gamma_j) \qquad (5)$$

where C (β) is defined as the outward deformation of the ring at $\Theta=\beta$ due to an outward unit load at $\Theta=0$.

Here, the terms $C_I(\beta)$ are referred to as influence coefficients of the ring and their explicit form may be found in the published literature [18].

Similarly, the effect of reaction loading upon housing deformation is computed as

$$D_o(\beta) = \sum_{j=1}^{n} G_j C_o(\beta-\gamma_j) \tag{6}$$

where $C_o(\beta)$ carries an analogous definition to $C_I(\beta)$. Note that the influence coefficients for a housing of completely arbitrary geometry can be obtained by the use of a finite element analysis.

Additional constraints are needed now to confine the deformed ring shape within the physical boundaries of the deformed housing. Having defined the set of $\bar{n}$ angles of interest, $\theta_j (j=1,\bar{n})$, the problem is reduced to one in which we must find a subset of indices, ℓ_k (k=1,n') such that

$$\text{at } \phi_k = \theta_{\ell_k}: \; D_o - D_I + \Delta = 0; \; k = 1,n' \tag{7}$$

and at all other angles, $\phi_k = \theta_j$:

$$D_o - D_I + \Delta > 0; \; j = 1,\bar{n}, \; j \neq \ell_k \tag{8}$$

where Δ is the clearance between the undeformed ring outer surface, whose center is displaced to coordinates (x_I, y_I), and the housing:

$$\Delta = R_o (1 + e_o \cos n_o (\theta - \Phi_o)) - R_I (1 + e_I \cos n_I (\theta - \Phi_I)) + x_I \cos\theta + y_I \sin\theta \tag{9}$$

Equations (5) through (9) are combined and evaluated at an angle β to yield

$$D_o - D_I + \Delta = \sum_{j=1}^{n} G_j C_o(\beta - \Theta_{\ell_k}) - \sum_{i=1}^{m} F_i C_I(\beta - \phi_i) + \sum_{j=1}^{n} G_j C_I(\beta - \Theta) + R_o(1 + e_o \cos(n_o \beta)) - R_I(1 + e_I \cos(n_I \beta)) + x_I \cos\beta + y_I \sin\beta \quad (10)$$

When a set of ℓ_k (k=1,n') is assumed, equation (10) evaluated at $\beta=\Theta_{\ell_i}$ (i=1,n') and equated to zero and equations (3) and (4) with $\gamma_k=\Theta_{\ell_k}$ form a set of n'+2 linear equations in the n'+2 unknowns G_k(k=1,n'), x_I and y_I. After solution of that set of equations, we must check that all G_k (k=1,n') are positive; then equation (8) must be checked at all Θ_j with j=1,$\bar{n}$ and with $j \neq \ell_k$ (k=1,n') and must be positive.

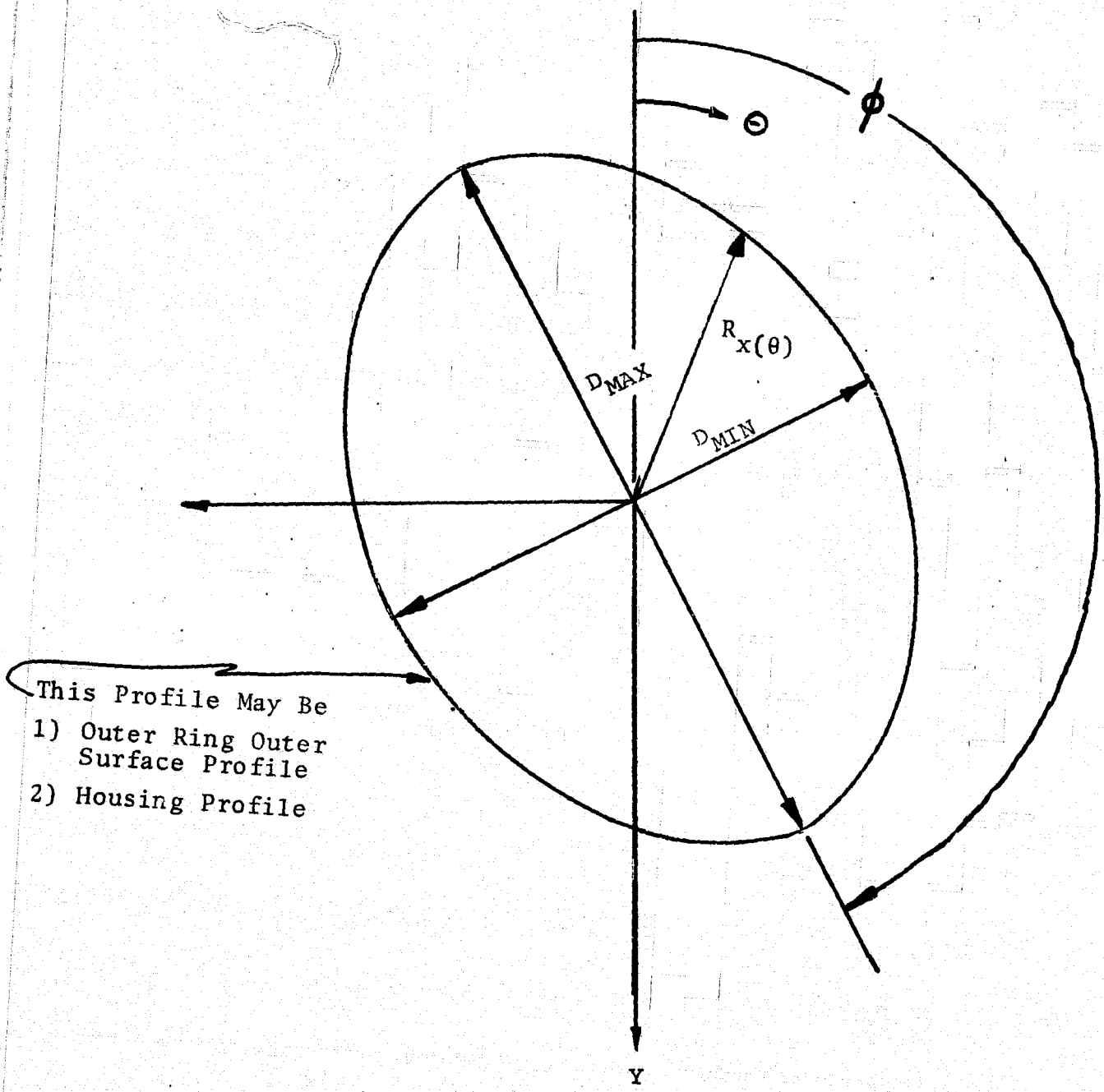

FIGURE F-1: NON-CIRCULAR PROFILE DESCRIPTION

APPENDIX G

GOVERNING EQUATION SET
AND
SOLUTION ALGORITHM

VOLUME I

APPENDIX G: GOVERNING EQUATION SET AND SOLUTION ALGORITHM

EQUATIONS OF EQUILIBRIUM

The determination of roller, ring and cage loading detail during operation, requires that the representation of these components satisfy equations of force and moment equilibrium. A total of $6n_r + 5$ equations may be formulated.

The formulation of the equations of equilibrium in turn, frequently requires the specification of a force or moment in a coordinate frame different from the one in which it was originally determined. This is accomplished by vector manipulation and the use of the transformation operators described in Appendix B.

INNER RING EQUILIBRIUM EQUATIONS

The computation of roller contact elastic and friction forces enables the writing of inner ring equilibrium equations by the summation of these loads over all rolling element locations i:

$$\sum_{i=1}^{n_r} \left[\sum_{k=1}^{n} \left(\{\bar{F}^i_{k,2} + \bar{T}^i_{k,2}\}_I \right) + \sum_{e=1}^{2} \left(\{\bar{f}^i_e\}_I \right) \right] + \{\bar{F}_A\}_I = 0 \qquad (1)$$

$$\sum_{i=1}^{n_r} \left[\sum_{k=1}^{n} \left(\{\bar{M}^i_{k,2} + \bar{U}^i_{k,2}\}_I \right) + \sum_{e=1}^{2} \left(\{\bar{m}^i_e\}_I \right) \right] + \{\bar{M}_A\}_I = 0 \qquad (2)$$

Here, $\{\bar{F}_A\}_I$ and $\{\bar{M}_A\}_I$ represent the specified applied loading.

Hydrodynamic loading is excluded from this equation set because of its extremely small magnitude when compared with contact and applied loads. The six vector component equations (1) and (2) with the appropriate imposed boundary values define the inner ring equilibrium field equation set. However, in bearing design analysis it is very convenient to specify the radial components of $\{\bar{F}_A\}_I$ and a misalignment angle. In this case the moments $\{\bar{M}_A\}_I$, decouple from Equation (2) and consequently may be evaluated directly. The remaining equations of equilibrium are reduced to the Y_I and Z_I components of (1).

ROLLING ELEMENT EQUILIBRIUM EQUATIONS

The $(6n_r)$ rolling element equations of equilibrium are obtained by summing all forces and moments applied to the i-th roller as follows:

$$\sum_{m=1}^{2}\left(\sum_{k=1}^{n}\{\bar{F}^i_{k,m}+\bar{T}^i_{k,m}\}_{\bar{R}}\right)+\sum_{e=1}^{2}(\{f^i_e\}_{\bar{R}})+ \tag{3}$$

$$\{\bar{F}^i_c\}_{\bar{R}}+\{\bar{H}^i\}_{\bar{R}}+\{\bar{F}^i_q\}_{\bar{R}}+\{\bar{F}^i_{Drag}\}_{\bar{R}}=0$$

$$\sum_{m=1}^{2}\left(\sum_{k=1}^{n}\{\bar{M}^i{}_{k,m}+\bar{U}^i_{k,m}\}_{\bar{R}}\right)+\sum_{e=1}^{2}(\{\bar{m}^i_e\}_{\bar{R}})+ \tag{4}$$

$$\{\bar{M}^i_c\}_{\bar{R}}+\{\bar{G}^i\}_{\bar{R}}+\{\bar{M}^i_q\}_{\bar{R}}=0$$

CAGE EQUILIBRIUM EQUATIONS

The cage maintains equilibrium by balancing its pocket and land forces:

$$\sum_{i=1}^{n_r} [(-f_i) \sin\psi_i + (-F_i) \cos\psi_i] - W_y = 0 \qquad (5)$$

$$\sum_{i=1}^{n_r} [(-f_i) \cos\psi_i + (F_i) \sin\psi_i] - W_z = 0 \qquad (6)$$

$$M_x + \frac{d}{2} \sum_{i=1}^{n_r} (-f_i) - \sum_{i=1}^{n_r} M_c^i = 0 \qquad (7)$$

SOLUTION ALGORITHM

Several computation procedures, and hence several opportunities, exist for the economic calculation of values for the set of independent variables. In contrast to the generality maintained in the bearing analysis formulation, specific solution algorithms are required to address the specific problems arising during the computation of bearing performance detail. The following physical conditions make the field equation set particularly difficult to solve:

1) Contact/No-Contact - The rollers transmit force through physical contact with the outer and inner rings and one or more flanges. It is known that the rollers must at high speeds, contact at least the outer ring at all times (centrifugal force). However, similar knowledge of flange contact kinematics is unavailable, thus giving rise to very poor initial guesses of skew and axial position.

2) Piece-wise Continuity of Function Derivations - As a result of clearances in the bearing, such as roller end play and radial looseness, the governing equation set becomes piece-wise continuous in its derivatives. This is especially true of the inner ring, roller radial, skew moment and axial equilibrium equations.

3) Accuracy - Loss of accuracy, through round-off errors, is especially influential when computing approximations to the derivatives of the field equation set.

A solution algorithm was constructed which minimizes these problems. Equilibrium is sought through automated Newton-Raphson iteration. Automatic variable damping is included to eliminate oscillations in localized minima of the function hyperspace.

An automated field equation set partitioning scheme was developed so that many different subsets of equations and independent variables could be experimented with to determine an optimum solution algorithm. Experimentation with this partitioning scheme led to the isolation of axial displacement and roller skew as the most difficult variables to control, along with the axial and skew moment equilibrium equations, the most difficult to equilibrate. Field equations written in the standard "force-displacement" format could not be brought to numerical equilibrium.

This was caused by the high sensitivity of the flange induced force to variation in axial and skew positions. Large roller end radii need only very small penetration into the flange to yield high reactive forces.

To avoid this numerical problem, an alternate solution algorithm was devised. Raceway induced roller loading is computed in the usual manner using standard "force-displacement" relationships. The net axial raceway induced load, F_{NX}, required to produce equilibrium is obtained and specified to equal the axial component of the flange induced load. The contact side, right or left flange, is obtained by noting the sign of F_{NX}. Using the unit vector in the direction of the resulting flange force, which was given in Appendix E, along with the EHD traction model, a flange induced load vector and contact location is obtained. Moments are computed using the vector cross product.

The above calculated flange force vectors, together with the raceway induced forces, provide roller equilibrium in the axial direction. With this equilibrium obtained, the axial equilibrium equation is removed from the field equation set and replaced by the equivalent kinematic relationship which states that the flange penetration is zero (see Equation (15), Appendix E) i.e.:

$$\delta_1 = D_1 - r_s = 0 \tag{8}$$

Here, r_s is the roller end sphere radius and the numeric subscript refers to the specific side on which contact occurs.

Using the above algorithm, one establishes contact at one flange and satisfies axial equilibrium.

This algorithm was subsequently expanded to include two contacts. By comparison of the flange induced roller moment with raceway induced moments, one may distribute the flange induced loading between two flange contacts (if necessary) such that both axial and skew moment equilibrium is achieved.

Consequently, the skew moment equilibrium equation is dropped from the equation set and replaced by the equivalent kinematic equation:

$$\delta_2 = D_2 - r_s = 0 \qquad (9)$$

Full algorithm detail and logical options are shown in Figure G-1.

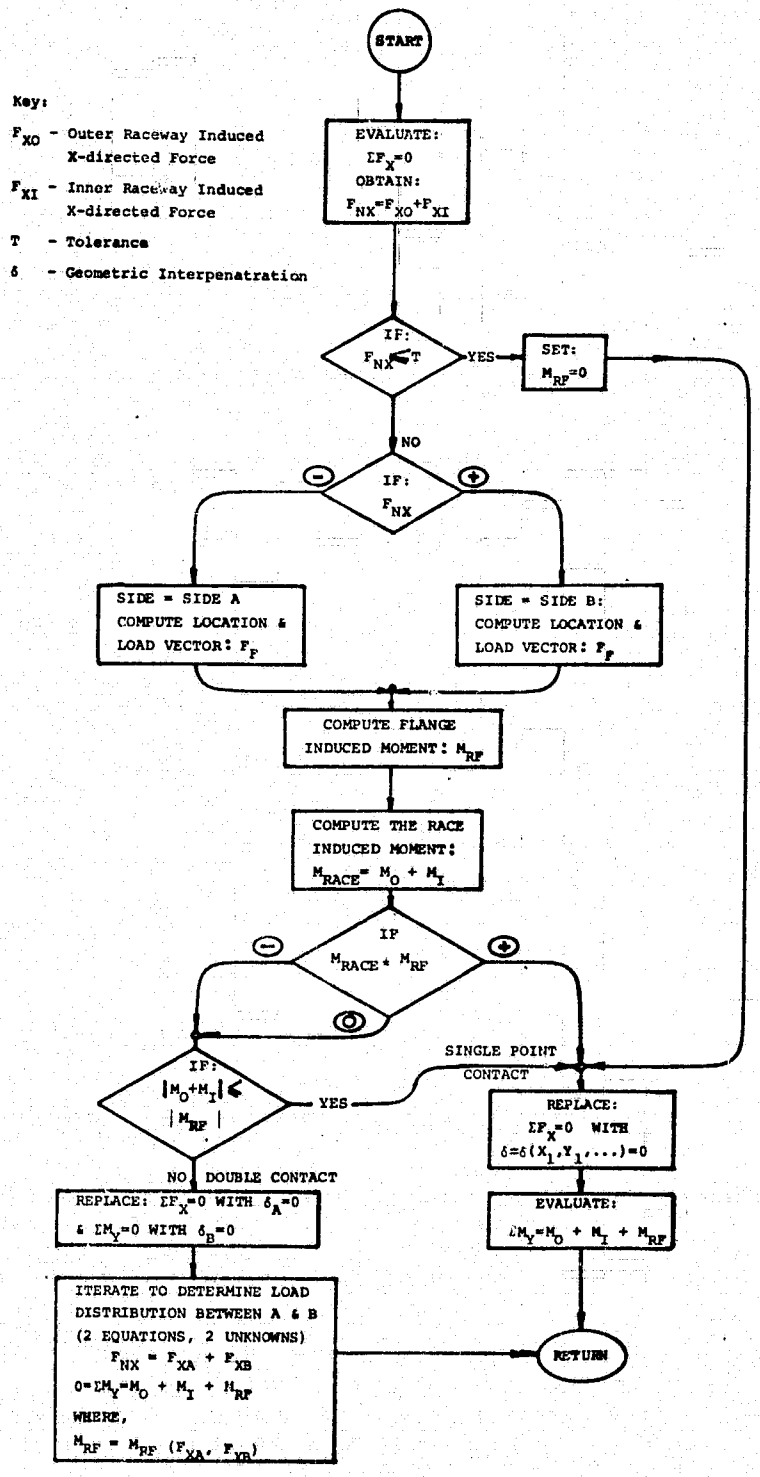

FIGURE G-1: SOLUTION ALGORITHM FOR MULTIPLE FLANGE CONTACTS

NOMENCLATURE

APPENDIX G

$F^i_{k,m}$	elastic roller/raceway contact load (lbs-see equation 6, Appendix E)
$T^i_{k,m}$	friction force at roller/raceway contact (lbs-see equation 40, Appendix E)
f^i_e	roller end/flange contact load (lbs)
$M^i_{k,m}$	elastic roller/raceway contact moment (in-lbs - see equation 8, Appendix E)
$U^i_{k,m}$	friction moment at roller/raceway contact (in-lbs - see equation 42, Appendix E)
m^i_e	friction moment at roller end/flange contact (in-lbs)
F^i_c	roller/cage web contact load (lbs - see equation 34, Appendix E)
H^i	hydrodynamic roller/raceway contact force (lbs - see equation 36, Appendix E)
F^i_q	quasidynamic roller force (lbs - see equation 48, Appendix E)
F^i_{Drag}	roller drag force (lbs - see equation 46, Appendix E)
M^i_c	moment generated by roller/cage web contact (in-lbs - see equation 35, Appendix E)
G^i	moment generated on roller by hydrodynamic forces (in-lbs - see equation 37, Appendix E)
M^i_q	quasidynamic roller moment (in-lbs - see equation 49, Appendix E)
f_i	radially directed cage pocket/roller contact friction force (lbs - see equation 32, Appendix E)
F_i	cage pocket/roller contact load (lbs - see equation 31, Appendix E)
W_y, W_z, M_x	cage/pilot surface forces (W_y, W_z-lbs) and moment (M_x-in-lbs) about cage axis of rotation (see equation 28, Appendix E)

$\{\overline{V}\}_{\alpha}$ a vector in the α coordinate system (coordinate frames are defined in Appendix B)

Subscripts/Superscripts

e refers to e-th flange, e = 1,2

i refers to i-th roller, i = 1,2,3,...,50

k refers to k-th slice (per Appendix E - Roller Raceway Forces) k = 1,2,3,...,20

m refers to m-th raceway, m=1 for outer ring, m=2 for inner ring

APPENDIX H

BEARING FATIGUE LIFE CALCULATIONS

VOLUME I

APPENDIX H: BEARING FATIGUE LIFE CALCULATIONS

INTRODUCTION

Within CYBEAN, roller bearing fatigue life is calculated using Lundberg-Palmgren [19,20] methods. The value computed is then modified by multiplicative factors which account for material and lubrication effects.

ROLLER BEARING RACEWAY LIFE

The Load distribution across a line contact is represented by a number of slices. The L_{10} fatigue life of a given slice is:

$$L_{10mk} = \left(\frac{Q_{cmk}}{Q_{emk}}\right)^4 \qquad (1)$$

Here, Q_{cmk} is defined as the load for which a slice will have 90 percent assurance of surviving 1 million revolutions. Letting m refer to a raceway, k to a slice, where n is the index of the last slice, the explicit form of Q_{cmk} is given by:

$$Q_{cmk} = \frac{49500\ \lambda\ \{D(1 \pm \gamma)\}^{1.074}\ \ell_m^{0.778}\ (\gamma_m)^{0.222}}{\{N(1 \mp \gamma_n)\}^{0.25}} \qquad (2)$$

Here, N is the number of rollers and, the upper sign is used for the outer race, the lower sign for the inner race.

Q_{emk} is the equivalent load for the slice:

$$Q_{emk} = \frac{1}{n_r}\left(\sum_{j=1}^{n_r} Q_{mkj}^{\varepsilon}\right)^{1/\varepsilon} \qquad (3)$$

Q_{mkj} is the individual roller contact load on the k-th slice and $\varepsilon = 4.0$ or $\varepsilon = 4.5$, depending respectively upon whether the applied load rotates or is stationary with respect to the raceway in question.

L_{10} life of a raceway is given by

$$L_{10m} = a_2 \, a_3 \, a_3^* \, a_4 \left\{ \sum_{k=1}^{n} L_{10mk}^{-e} \right\}^{-1/e} \qquad (4)$$

where e is the Weibull slope exponent, here taken to be 9/8

a_2 is a life improvement factor to account for improved materials

a_3 is a life improvement factor to account for full film lubrication

a_3^* is less than 1 when full film lubrication is not obtained [21].

a_4 is a factor which accounts for materials having a modulus of elasticity other than that of basic steel.

BEARING LIFE

L_{10} life of the bearing considering both raceways is:

$$L_{10} = \left\{ \sum_{m=1}^{2} (L_{10m})^{-e} \right\}^{-1/e} \qquad (5)$$

NOMENCLATURE

APPENDIX H

γ	D/d_m
D	roller diameter (in)
d_m	pitch diameter (in)
ℓ	slice width (in)
λ	capacity reduction factor λ_k = .8 when K=2,3,...,(N-1) λ_k = .53 when K=1 or N, N=Number of slices
n_r	number of rollers

APPENDIX I

THERMAL MODEL

VOLUME I
APPENDIX I: THERMAL MODEL

TEMPERATURE CALCULATIONS

After each calculation of bearing generated heat rates, either steady state or time transient temperature analysis may be performed. The computations are terminated in the following manner:

1. The steady state case terminates when each system node temperature is within Δ °Centigrade of its previously predicted value, The value for Δ is specified by the user.

2. The transient calculation terminates when the user specified computation time is reached or when one of the system temperature nodes exceeds 600°C (1112°F).

STEADY STATE TEMPERATURE MAP

The physical structure is considered to be divided into a number of elements represented by nodes. Heat flow to node i from surrounding nodes j, plus the heat generated at node i, must equal zero to satisfy the definition of steady state conditions.

After each calculation of bearing generated heat, which results from a solution of the bearing portion of the program, a set of system temperatures is determined which satisfy:

$$q_i = q_{oi} + q_{gi} = 0 \text{ for all nodes } i \qquad (1)$$

where q_{oi} is the heat flow from all neighboring nodes to node i

q_{gi} is the heat generated at node i. Values are calculated to represent heat created by bearing friction.

The resulting set of field equations is solved with a modified Newton-Raphson method which successfully terminates when either:

$$\frac{\Delta t_i}{t_i} \leq \delta \text{ for all nodes } i \qquad (2)$$

here, Δt represents the Newton-Raphson correction to the i-th temperature.

or: $$\frac{1}{100} \sum_{i=1}^{n} \left[\frac{(EQ)_i^2}{n} \right]^{1/2} \leq \delta \qquad (3)$$

where, n = number of field equations
EQ_i = residue of the i-th field equation
δ = .001

TRANSIENT TEMPERATURES

The net heat q_i transferred to the i-th node heats the element, i.e.:

$$\rho C_{p_i} V_i \frac{dt_i}{dT_i} = q_i \qquad (4)$$

where ρ = density
C_p = specific heat
V = volume of the element
t = temperature
T = time

The temperatures, t_{oi}, at the time of initiation $T=T_s$ are assumed to be known, that is

$$t_{oi} = t_i (T_s) \qquad i = 1, 2, \ldots, n \qquad (5)$$

The problem of calculating the transient temperature distribution in a bearing configuration thus becomes a problem of solving a system of nonlinear differential equations of the first order with prescribed initial conditions. The equations are nonlinear since they contain radiation terms and free convection, which are nonlinear with temperature as will be shown later. The simplest and most economical way to arrive at a solution is to calculate the rate of temperature increase at the time $T = T_k$ from equation (4) and then compute the temperatures at time $T_k + \Delta T$ from

$$t_{k+1} = t_k + \frac{dt_k}{dT} \Delta T = t_k + \frac{q_k}{\rho C_p V} \Delta T \qquad (6)$$

CALCULATION OF TRANSIENT TIME STEP

If the time step ΔT used is chosen too large, the temperatures will oscillate; if it is chosen too small the calculation will be costly. It is therefore desirable to choose the largest possible time step that does not give an oscillating solution [22,23].

$$\frac{dt_{i,k+1}}{dt_{i,k}} \geq 0 \qquad i = 1,2,\ldots, n \qquad (7)$$

If this derivative were negative, the implication would be that the local temperature at node i has a negative effect on its future value. This would imply that the hotter a region is now, the colder it will be after an equal time interval. Oscillating solution would result.

Differentiating (6) for node i and combining with (7), the time step size condition is

$$\frac{dt_{i,k+1}}{dt_{i,k}} = 1 + \frac{\Delta T_i}{\rho_i C_{p_i} V_i} \frac{dq_i}{dt_i} \geq 0 \qquad (8)$$

The derivative dq_i/dt_i is approximated using the forward difference operator

$$\frac{dq_i}{dt_i} = \frac{q_i(t_i + \Delta t_i) - q_i(t_i)}{t_i} \qquad (9)$$

The values ΔT_i which satisfy the equality in Equation (8) are calculated. The array is searched, and a value of ΔT rounded off to one significant digit smaller than the smallest of the ΔT_i obtained is used.

CALCULATION OF HEAT TRANSFER RATE

Heat transfer mechanisms which occur in a bearing application are:

- Conduction between inner ring and shaft and between outer ring and housing.
- Convection between the surface of the housing and the surrounding air.
- Radiation between the shaft and the housing.
- Forced convection between the bearing and circulating oil.

All the above mentioned modes of heat transfer are considered in calculations of the heat balance at each given node.

GENERATED HEAT

A heat source may exist at node i. The quantity representing the source magnitude must be added to the net heat flowing from neighboring nodes.

When the heat source is other than a cylindrical roller bearing, it may be considered to produce known amounts of power, in which case constant numbers are entered as input to the program (see example in Volume II).

CONDUCTION

The heat flow $q_{ci,j}$ which is transferred by conduction from node i to node j, is:

$$q_{ci,j} = \frac{\lambda A}{\ell} (t_i - t_j) \qquad (10)$$

where λ = the thermal conductivity of the medium.
ℓ = length between i and j

FREE CONVECTION

Free convection between a solid medium and air, the heat flow $q_{vi,j}$ transferred between nodes i and j can be calculated from the equation

$$q_{vi,j} = \alpha_v A \mid t_i - t_j \mid^d \cdot \text{SIGN}\ (t_i - t_j) \qquad (11)$$

where

α_v = the film coefficient of heat transfer by free convection

A = the surface area of thermal contact between the media

d = is an exponent, usually = 1.25, but any value can be specified as input to the program

$$\text{SIGN} = \begin{cases} 1 \text{ if } t_i \geq t_j \\ -1 \text{ if } t_i \leq t_j \end{cases}$$

The value of α_v can be calculated for various cases [22].

FORCED CONVECTION

Heat flow $q_{wi,j}$ transferred by forced convection can be obtained from the following equation.

$$q_{wi,j} = \alpha_w A(t_i - t_j) \qquad (12)$$

where α_w is the film coefficient of heat transfer during forced convection. This value is dependent on the actual shape, the surface condition of the body, the difference in speed, as well as the properties of the liquid or gas.

In most cases, it is possible to calculate the coefficient of forced convection from a general relationship of the form,

$$N_u = aR_e^b P_r^c \qquad (13)$$

where a, b, and c are constants obtained from handbooks, [24],
R_e and P_r are dimensionless numbers defined by

N_u = Nusselt number = $\alpha_w L/\lambda$
L = characteristic length
λ = conductivity of the fluid
R_e = Reynold's number = $UL\rho/\eta$
U = characteristic speed
ρ = density of the fluid
η = dynamic viscosity of the fluid
P_r = Prandtl's number = $\eta C_p/\lambda$
C_p = specific heat

CYBEAN can accept a specified constant value for the coefficient of convection, or, let it vary with actual temperatures. The variation is determined by the viscosity variation. Input can be given in one of three ways, for each coefficient.

Constant Viscosity

1. Values of the parameters in Equation (13) are given as input and a constant value of α_w is calculated by the program.

Temperature Dependent Viscosity

2. The coefficient α_w for turbulent flow and heating of petroleum oils is given by

$$\alpha_w = k_g \cdot \{\eta\ (t)\}^{k_{10}} \qquad (14)$$

where k_g and k_{10} are given as input together with viscosity at two different temperatures.

3. Values of the parameters in Equation (13) are given as input. Viscosity is given at two different temperatures.

RADIATION

If two flat, parallel surfaces of same surface area A, are placed close together, the heat transferred by radiation between nodes i and j representing those bodies, will be,

$$q_{Ri,j} = \varepsilon\sigma A\ [(t_i + 273)^4 - (t_j + 273)^4] \qquad (15)$$

here, ε is the surface emissivity, and σ is the Stefan-Boltzmann radiation constant.

Heat transfer by radiation under other conditions can also be calculated [22]. The following equation, for instance, applies between two concentric cylindrical surfaces:

$$q_{Ri,j} = \frac{\varepsilon\sigma A_i\ [(t_i + 273)^4 - (t_j + 273)^4]}{1 + (1-\varepsilon)\ (A_i/A_e)} \qquad (16)$$

where A_i is the area of the inner cylindrical surface
A_e is the area of the outer cylindrical surface

FLUID FLOW

Between nodes established in fluids, heat is transferred by transport of the fluid itself and the heat it contains.

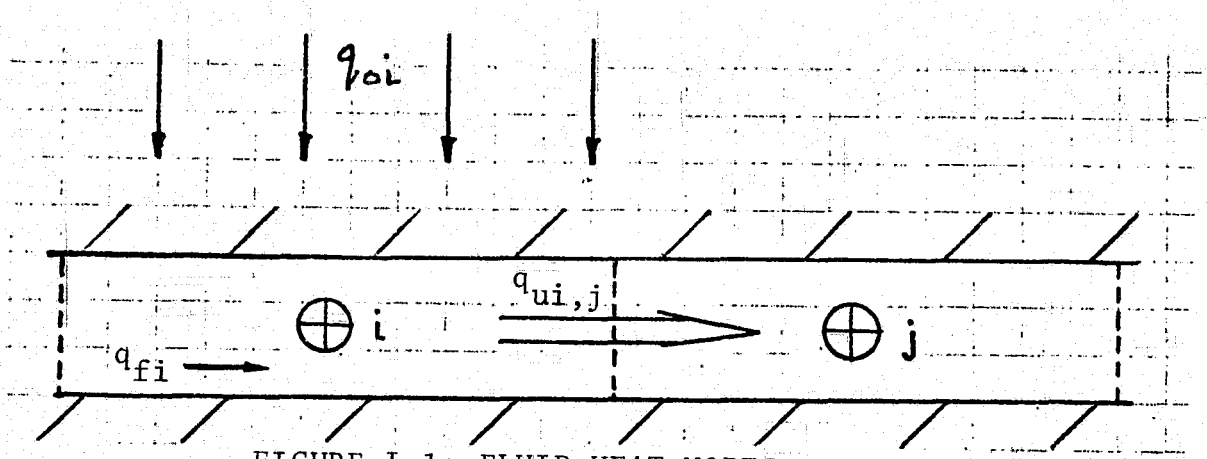

FIGURE I-1: FLUID HEAT NODES

Figure I-1 shows nodes i and j at the midpoints of consecutive segments established in a stream of flowing fluid.

The heat flow $q_{ui,j}$ through the boundary between nodes i and j can be calculated as the sum of the heat flow q_{fi} through the middle of the element i, and half the heat flow q_{oi} transferred to node i by other means, eg., convection.

The heat carried by mass flow is,

$$q_{fi} = \rho_i C_{p_i} V_i t_i = K_i t_i \qquad (17)$$

where V_i = the volume flow rate through node i.

The heat input to node i is the sum of the heat generated at node i (if any) and the sum over all other nodes of the heat transferred to node i by conduction, radiation, free and forced convection.

$$q_{oi} = q_{G,i} + \sum_j (q_{ci,j} + q_{vi,j} + q_{wi,j} + q_{Ri,j}) \quad (18)$$

The heat flow between the nodes of Figure I-1 is then,

$$q_{ui,j} = q_{fi} + q_{oi}/2 \quad (19)$$

If the flow is dividing between node i and j, as in Fig. I-2, then the heat flow is calculated from

$$q_{ui,j} = K_{ij} (q_{fi} + q_{oi}/2) \quad (20)$$

where K_{ij} = the proportion of the flow at i going to node j,
$0 \leq K_{ij} \leq 1$.

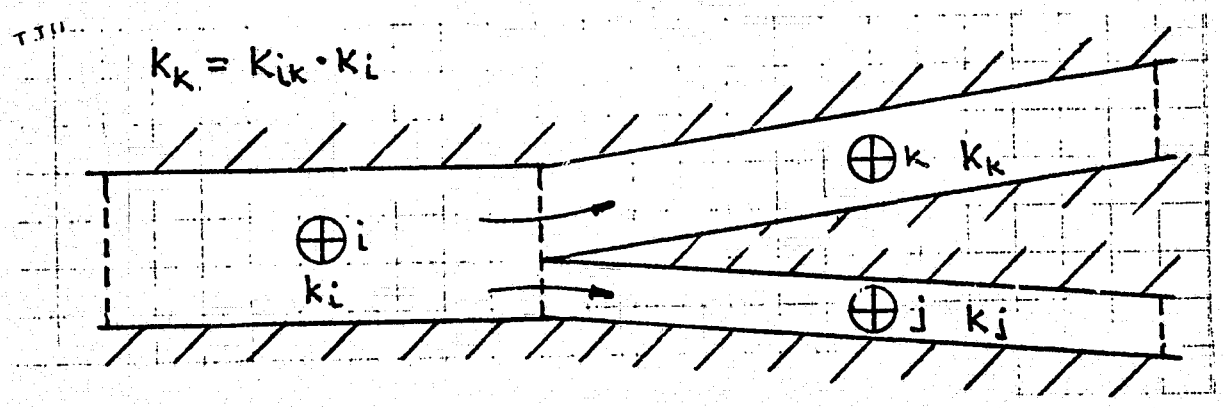

FIGURE I-2: DIVIDED FLUID FLOW FROM NODE i

TOTAL HEAT TRANSFERRED

The net heat flow rate to node i can be expressed as,

$$q_i = q_{G,i} + \sum_j (q_{ci,j} + q_{ui,j} + q_{vi,j} + q_{wi,j} + q_{Ri,j}) \quad (21)$$

The summation should include all nodes j, which interact with i. Unknown temperatures as well as those specified as known should be included.

CONDUCTION THROUGH A BEARING

The conduction between two nodes is governed by the thermal conductivity parameter λ. The value of λ is specified at input.

An exception occurs when one of the nodes represents a bearing ring and the other a set of rolling elements. Here, the conduction is calculated separately using the principles described below.

THERMAL RESISTANCE

It is assumed that the rolling speeds of the rolling elements are so high that the bulk temperature of the rolling elements is the same at both the inner and outer races, except in a volume close to the surface. The resistance to heat flow can then be calculated as the sum of the resistance across the surface and the resistance of the material close to the surface.

The resistance Ω is defined implicitly by

$$\Delta t = \Omega \cdot q \qquad (22)$$

where Δt is the temperature difference
and q is the heat flow

The resistance due to conduction through the EHD film is calculated as

$$\Omega_1 = (h/\lambda) \cdot A \qquad (23)$$

where h is taken to be the calculated plateau film thickness

A is the Hertzian contact area at the specific rolling element-ring contact under consideration.

λ is the conductivity of the oil.

The geometry is shown in Figure I-3(a). Asperity conduction is not considered.

So far, a constant temperature difference between the surfaces has been assumed. But during the time period of contact, the difference will decrease because of the finite thermal diffusivity of the material near the surface, Figure I-3(b).

To points at a distance from the surface, this phenomenon will have the same effect as an additional resistance Ω_2 acting in series with Ω_1.

This resistance was estimated [25] as,

$$\Omega_2 = \frac{1}{\lambda \ell_{re,i}} \left(\frac{\pi\psi}{2b_i V}\right)^{1/2} \qquad (24)$$

where ℓ_{re} = contact length, or in the case of an elliptical contact area, 0.8 times the major axis

λ = heat conductivity

ψ = thermal diffusivity = $\lambda/(\rho \cdot C_p)$

ρ = density

C_p = specific heat

b = half the contact width

V = rolling speed

The resultant resistance is

$$\Omega_{res} = \Omega_1 + \Omega_2 \qquad (25)$$

There is one such resistance at each rolling element. They all act in parallel. The resultant resistance, Ω_{res}, is thus obtained from

$$\frac{1}{\Omega_{res}} = \sum_{i=1}^{\eta} \frac{1}{\Omega_{res,i}} \qquad (26)$$

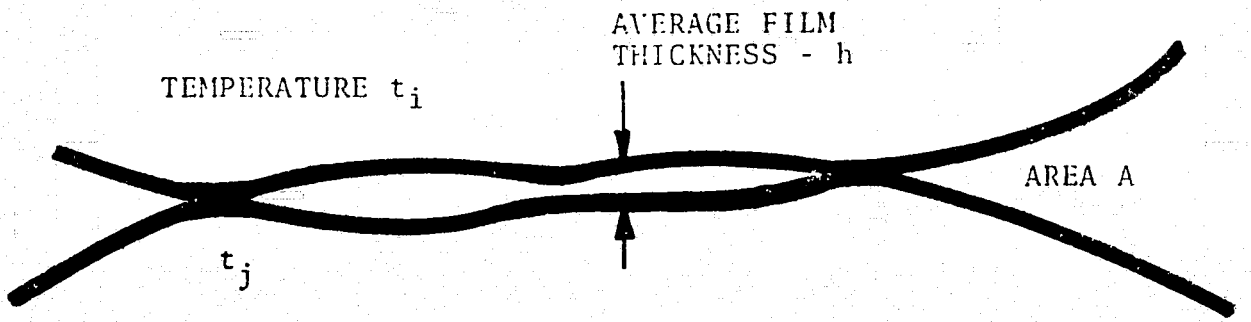

(a) Schematic Concentrated Contact

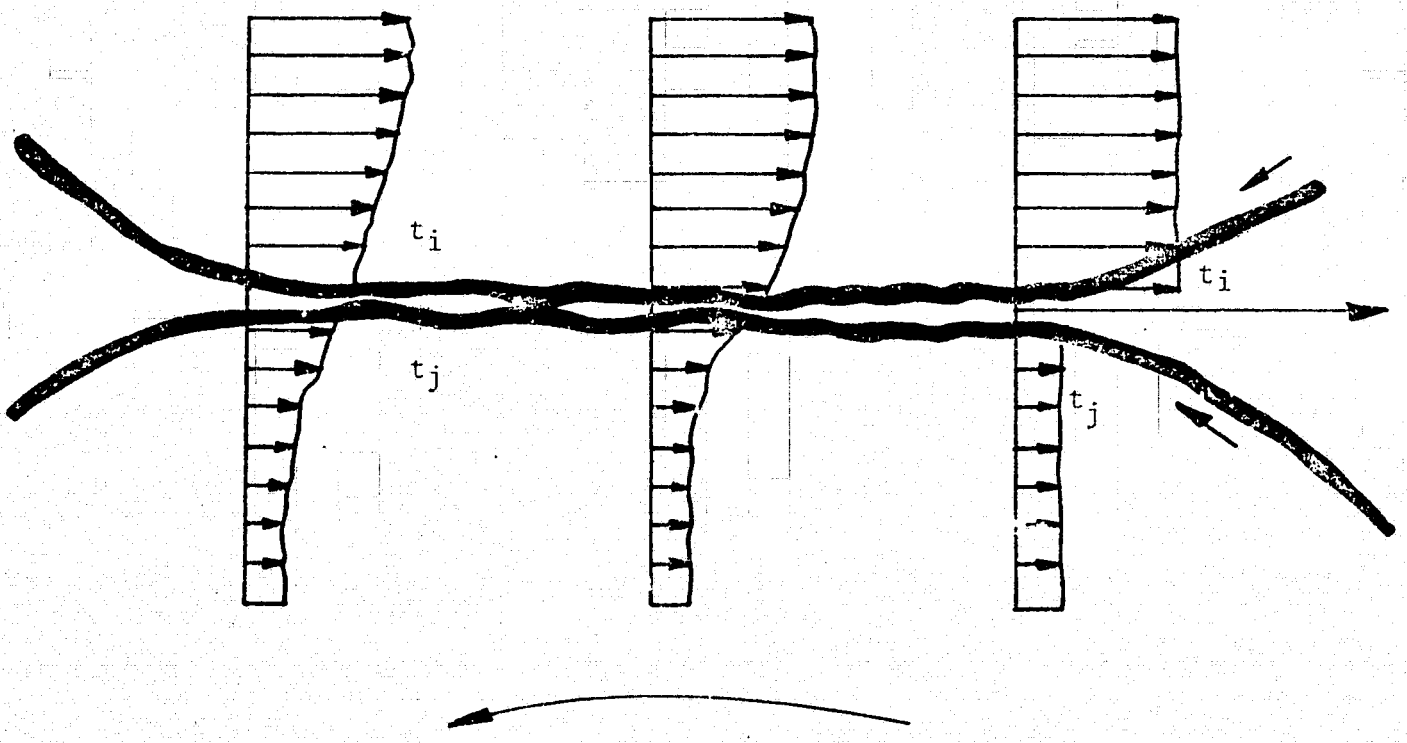

(b) Temperature Distribution at Rolling, Concentrated Contact Surfaces

FIGURE I-3: CONTACT GEOMETRY AND TEMPERATURES

REFERENCES

1. Liu, J. Y., "The Effect of Misalignment on the Life of High Speed Cylindrical Roller Bearings," TRANS. ASME, JOLT, January, 1971, pp. 60-68.

2. Goldstein, H., "Classical Mechanics," Addison Wesley, 1965, pp. 93-109.

3. McGrew, J. M., et al, "Elastohydrodynamic Lubrication Preliminary Design Manual," Technical Report AFAPL-TR-70-27, pp. 20-21, November 1970.

4. Fresco, G. P., et al, "Measurement and Prediction of Viscosity-Pressure Characteristics of Liquids," A Thesis in Chemical Engineering Report No. PRL-3-66, Dept. of Chemical Engineering, College of Engineering, The Penna. State University, University Park, Penna.

5. Lundberg, G., "Cylinder Compressed Between Two Plane Bodies," SKF Internal Report, 1949-08-02.

6. Boness, R. J., "The Effect of Oil Supply on Cage and Roller Motion in a Lubricated Roller Bearings," Trans. ASME, Journal of Lubrication Technology, January 1970, pp. 39-53.

7. Harris, T. A., "Rolling Bearing Analysis," John Wiley and Sons, pp. 321-327.

8. Poplawski, J. V., "Slip and Cage Forces in a High Speed Roller Bearing," Journal of Lubrication Technology, Trans. ASME, Series D, Vol. 94, No. 2, April 1972, pp. 143-152.

9. Pinkus, O. and Sternlecht, B., "Theory of Hydrodynamic Lubrication," McGraw-Hill, pp. 48, 1961.

10. Dowson, D. and Higginson, G. R., "Elasto-Hydrodynamic Lubrication," Pergamon Press, 1966, p 41.

11. McCool, J. I., et al, Technical Report AFAPL-TR-75-25, "Influence of Elastohydrodynamic Lubrication on the Life and Operation of Turbine Engine Ball Bearings - Bearing Design Manual," SKF Report No. AL75P014 submitted to AFAPL and NAPTC under AF Contract No. F33615-72-C-1467, Navy MIPR No. M62376-3-00007, May 1975.

12. Chiu, Y. P., "An Analysis and Prediction of Lubricant Film Starvation in Rolling Contact Systems," ASLE Trans., 17, pp. 23-35 (1974).

REFERENCES (Continued)

13. Crecelius, W. J. and Pirvics, J., "Computer Program Operation Manual on SHABERTH - a Computer Program for the Analysis of the Steady State and Transient Thermal Performance of Shaft Bearing Systems," SKF Report No. AL76P030, submitted to AFAPL and NAPTC under AF Contract No. F33615-76-C-2061, AFAPL-TR-76-90, Navy MIPR No. M62376-MP-00005, July, 1976, pp. I-6-11, I-6-22.

14. Allen, C. W., Townsend, D. P. and Zaretsky, E. V., "New Generalized Rheological Model for Lubrication of a Ball Spinning in a Nonconforming Groove," NASA Technical Note D-7280, National Aeronautics and Space Administration, Washington, DC, May 1973.

15. Loewenthal, S. H., Parker, R. J. and Zaretsky, E. V., "Correlation of Elastohydrodynamic Film Thickness Measurements for Fluorocarbon, Type II Ester and Polyphenal Ether Lubricants," NASA Technical Note D-7825, National Aeronautics and Space Administration, Washington, DC, November 1974.

16. Knudsen, J. G. and Katz, D. L., "Fluid Dynamics and Heat Transfer," McGraw-Hill, New York, pp. 311-315.

17. Kellstrom M., "A Computer Program for Elastic and Thermal Analysis of Shaft Bearing Systems," SKF Report No. AL74P004, submitted to Vulnerability Laboratory, U.S. Army Ballistics Research Laboratory, under Contract No. DAAD05-73-C-0011.

18. Liu, J. Y., and Chiu, Y. P., "Analysis of a Thin Elastic Ring Under Arbitrary Loading," Journal of Engineering for Industry, TRANS. ASME, August 1974, pp. 870-876.

19. Lundberg, G. and Palmgren, A., "Dynamic Capacity of Roller Bearings," ACTA POLYTECHNICA, Vol. 2, No. 4, 1952.

20. Lundberg, G. and Palmgren, A., "Dynamic Capacity of Roller Bearings," ACTA POLYTECHNICA, Vol. 1, No. 3, 1947.

21. Liu, J. Y., "Dependence of Beairng Fatigue Life on Film Thickness to Surface Roghness Ratio," ASLE TRANSACTIONS, pp. 144-152, May, 1974.

22. Jakob, M. and Hawkins, G. A., "Elements of Heat Transfer," Third Ed., John Wiley & Sons, Inc., 1957.

23. Dusinberre, G. M., "Numerical Analysis of Heat Flow," McGraw-Hill Book Co., 1949.

24. Kent's Mechanical Engineering Handbook - Power Volume, John Wiley & Son, Inc., 12th Edition, 1960, Chapter 3, p. 20.

25. Burton, R. A. and Staph, H. E., "Thermally Activated Seizure of Angular Contact Bearings," ASLE Trans. 10, pp. 408-417 (1967).

ATTACHMENT 1

Roller Bearing Specifications

Inner Race

Bore Dia.	mm (in)	118 (4.6457)
Raceway Dia.	mm (in)	131.66 (5.1834)
Flange Dia.	mm (in)	137.47 (5.4122)
Width	mm (in)	26.92 (1.060)
Groove Width	mm (in)	14.59 (..5746)
Flange Angle		.6 deg.

Outer Race

Outer Dia.	mm (in)	164.49 (6.4760)
Raceway Dia.	mm (in)	157.08 (6.1842)
Width	mm (in)	23.9 (.942)

Rollers

Diameter	mm (in)	12.65 (.4979)
Length-overall	mm (in)	14.56 (.5733)
-effective	mm (in)	13.04 (.5133)
-flat	mm (in)	8.40 (.3307)
Crown Radius	mm (in)	622.3 (24.5)
End Radius	mm (in)	381.0 (15.)
Number		28

Cage

Land Diameter	mm (in)	137.95 (5.4312)
Axial Pocket Clearance	mm (in)	.020(.0008)
Tangential Pocket Clearance	mm (in)	.221(.0087)
Single Ball Width	mm (in)	4.6 (.18)

Operating Conditions

Shaft Speed		20,000 rpm
Bearing Radial Load	4450 N	(1000 lb)
Oil Inlet Temperature	366.5K	(200°F)
Misalignment of Races		0 deg & .5 deg. & .75 deg.